(49)

The Estimation of Arctic Ice Thickness from Ambient Noise

by

Olga Chernets

Submitted to the Department of Ocean Engineering
in partial fulfillment of the requirements for the degree of

Master of Science in Ocean Engineering

at the

MASSACHUSETTS INSTITUTE OF TECHNOLOGY

September 1995

Author .....
Department of Ocean Engineering
June 26, 1995

Certified by .....
J. Robert Fricke
Assistant Professor
Thesis Supervisor

Accepted by .....
D. Carmichael
Chairman, Departmental Committee on Graduate Students

The Estimation of Arctic Ice Thickness from Ambient Noise

by

Olga Chernets

Submitted to the Department of Ocean Engineering
on June 26, 1995, in partial fulfillment of the
requirements for the degree of
Master of Science in Ocean Engineering

Abstract

An estimate of Arctic ice thickness from the acoustic emission of the ice plate is the goal of this study. The Arctic ice is related to the global climate processes and the global heat and water budget. The focus of the thesis is the passive estimation of ice thickness using ambient noise caused by thermal and mechanical stress cracks in the ice sheet. An analytical model for a propagating crack in an ice plate is developed. According to the model, the acoustic signal received from propagating stress cracks is the convolution of an elemental fracture source function and the spatial distribution function (array). This analytic result predicts the spectral peak on the order of 1kHz that relates directly to the ice thickness. Experimental hydrophone data collected in the Beaufort Sea during the spring of 1994 demonstrates the presence of these spectral peaks, which correlate well with the measured ice thickness at the site. In addition, hydrophone observations of the sound generated by ice cracking events provide an opportunity for studying the sound waves which occur in the ice plate. The effects of the dispersion of Lamb waves and the attenuation of Lamb waves as a function of frequency for the parameters of an Arctic ice plate are obtained numerically and demonstrated by the experimental hydrophone data.

Thesis Supervisor: J. Robert Fricke
Title: Assistant Professor

Acknowledgments

I would like to thank my advisor, Rob Fricke, for his encouragement and support. It has been a most enjoyable experience to have opportunity to work with him. This work would not have been possible without his ideas and help on every step.

Also I would like to thank Dr. Lyon for introducing me to Arctic acoustic group and teaching me structural acoustics.

My special thanks go to Jane Dunphy, my English teacher, for her encouragement and support. I would like to thank her for having spent some extra time to correct my thesis even when she was in hurry with her own work.

All my office mates always were ready to give me an advice. Their understanding acoustics problems as well as computer experience were a great help.

My sincerest thanks go to my family for love and support. The thesis dedicated to my grandfather, G. S. Veksler, who always believed in my ability for engineering research.

Contents

List of Figures

List of Tables

Chapter 1

Introduction

1.1 Background

The Arctic is a principal area for ice research because of its role in the global climate and heat budget and its economical resources. One of the important parameters of the Arctic is the mass of the ice plate. For determination of the total ice mass, measurements of the ice thickness at numerous points of the ice plate should be provided. Direct measurements are obviously expensive.

Some indirect methods are known. Crissman [2] presents the method of calculating an ice thickness term using observed ice motion and wind data. The theory states that as wind blows over an ice parcel, the energy of the wind is transferred to and through the ice, and the ice moves.

Lewis gives another interesting approach in Ref. [3]. Thermal tension, and on a large scale, the effects of wind and current, can build up internal stress within the ice to the point at which it will rupture. In Ref. [3] thermally-induced stresses within ice floes are simulated using a visco-elastic model that accounts for the time variation of the atmospheric forcing parameters and the temporal and spatial variations of snow cover. To relate the model-predicted stresses to the observed 500 Hz under-ice noise variations, a fracturing paradigm was developed. The results indicate the connection between under-ice noise episodes and tensile fracturing of the ice pack. However, it is not clear from this work how to estimate ice thickness by analyzing under-ice noise.

As a complement to these efforts, the research described in this thesis is focused on estimating ice thickness through the spectral analysis of acoustic emissions from the ice plate. The sound field in the Arctic Ocean is the summation of many different source mechanisms. For understanding which of these mechanisms has the best correlation with ice thickness, physics of Arctic ice behavior is discussed below.

A primary source of sound in the Arctic Ocean arises from the response of the ice cover to stress. Temperature changes, wind, and current produce internal stress within the ice to the point of cracking. The visible consequences are cracks, pressure ridges, buckling, and fragmentation. Catastrophic failure of the ice during these events generates sound waves. In effect, the sudden displacement at the fracture zone excites various elastic waves in the ice, and some of this energy, together with the directly transmitted signal, enters the water, contributing to the ambient sound levels of the ocean. The problem is that the noise, say recorded by a hydrophone, is a superposition of many modes from numerous cracks and other sound sources. Therefore, it is not easy to identify which event in the noise corresponds to which mode.

Experimental results provide the information about the ambient noise as follows. According to Ref. [7], the noise power spectral density under the Arctic ice cap has a broad peak centered near 10Hz with approximately ω^{-2} slope above the peak, and a less well-defined slope below the peak. In Ref. [8] additional peaks at higher frequencies are also observed.

The sound generated by ice cracking events in the Amundsen Gulf is observed by Farmer and Xie in Ref. [9]. Contributions from waves traveling in the ice are identified and shown to be small compared to the direct acoustic wave. A feature of Farmer's experiment was that measurements were extended up to a frequency of 20kHz, revealing previously unidentified high-frequency components of the signal.

Analytical results about sound generation and propagation in sea ice also provide some insight. In Ref. [4] the field of a point source of compressional waves in the ice is computed. In Ref. [5] the crack is modeled by an approximate equivalent source, and the example shown represents a small fraction of the ice sheet under

tension. It is demonstrated that if the ice sheet were completely continuous, only a very small fraction of the energy released by the crack could be trapped as sound in the surface half-channel of the ocean, where it will contribute to the ambient noise. The interesting model proposed in Ref. [6] describes a crack in the ice plate as a combination of different types of seismic sources. Analytical solutions are developed for tensile crack, dip-slip and strike-slip.

In summary, previous research has provided the following relevant information:

1. The primary source of sound in the Arctic Ocean arises from the response of the ice cover to stress.

2. Only a small fraction of the total energy released in the "compact" cracking process is radiated at grazing angles of less than 15^o. It is difficult to get the information about ice from "compact" cracks.

3. The *most common* crack is a tensile fault, including the very fine cracks due to thermal tension acting over a cold surface skin and *larger cracks fracturing the ice over its full depth.*

4. *Direct acoustic transmission* dominates in the observed hydrophone signals of ambient noise.

1.2 Objective

The goal of the present research is to estimate ice thickness by analyzing the acoustic emission from the Arctic ice. The research effort in this thesis focuses on the modelling of the physical process of radiation from the propagating cracks, which fracture the ice over its full depth. Experimental hydrophone data collected in the Beaufort Sea during the spring of 1994 are analyzed to determine the ice thickness using this analytical model.(See Fig.1.1.) Furthermore, the effect of the Lamb waves on the acoustic emission is considered.

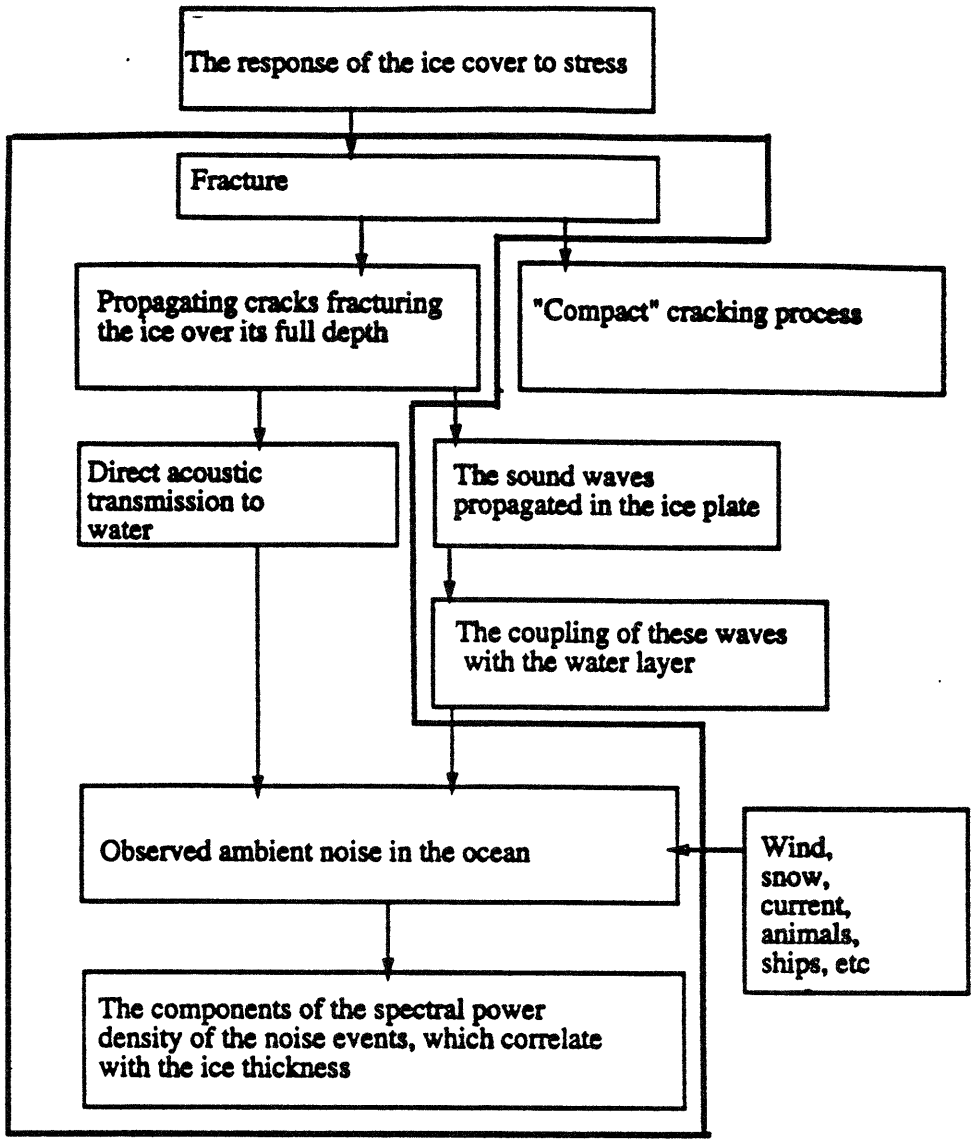

Figure 1-1: The research issues relating to the estimation of the ice thickness from the ambient noise. The topics that inside the large box are considered in the thesis.

1.3 Approach

The approach taken in the estimation of ice thickness from the ambient noise is divided into two parts:

- the development of a mathematical representation of a propagating crack,
- the creation of a numerical method for the spectral analysis of experimental hydrophone data.

The approach taken in analyzing the part of ambient noise events which comes from the modes of the waves propagating in the ice plate (Lamb waves) is based on the theory of elastic waves in an infinite solid layer.

The key point of this research, as shown in Fig.1.2, is that the observations of the noise events show similarities to seismic signals. This has motivated the approach to the modeling in which I adapt a theory of earthquake mechanics for the case of an ice plate. Another important point is that a propagating crack can be studied as a linear array of sources. The theory of sound radiation from linear arrays of sources will be used.

The signal from cracks is very short in time. The method of spectral analysis chosen for this research is the Maximum Likelihood Method.

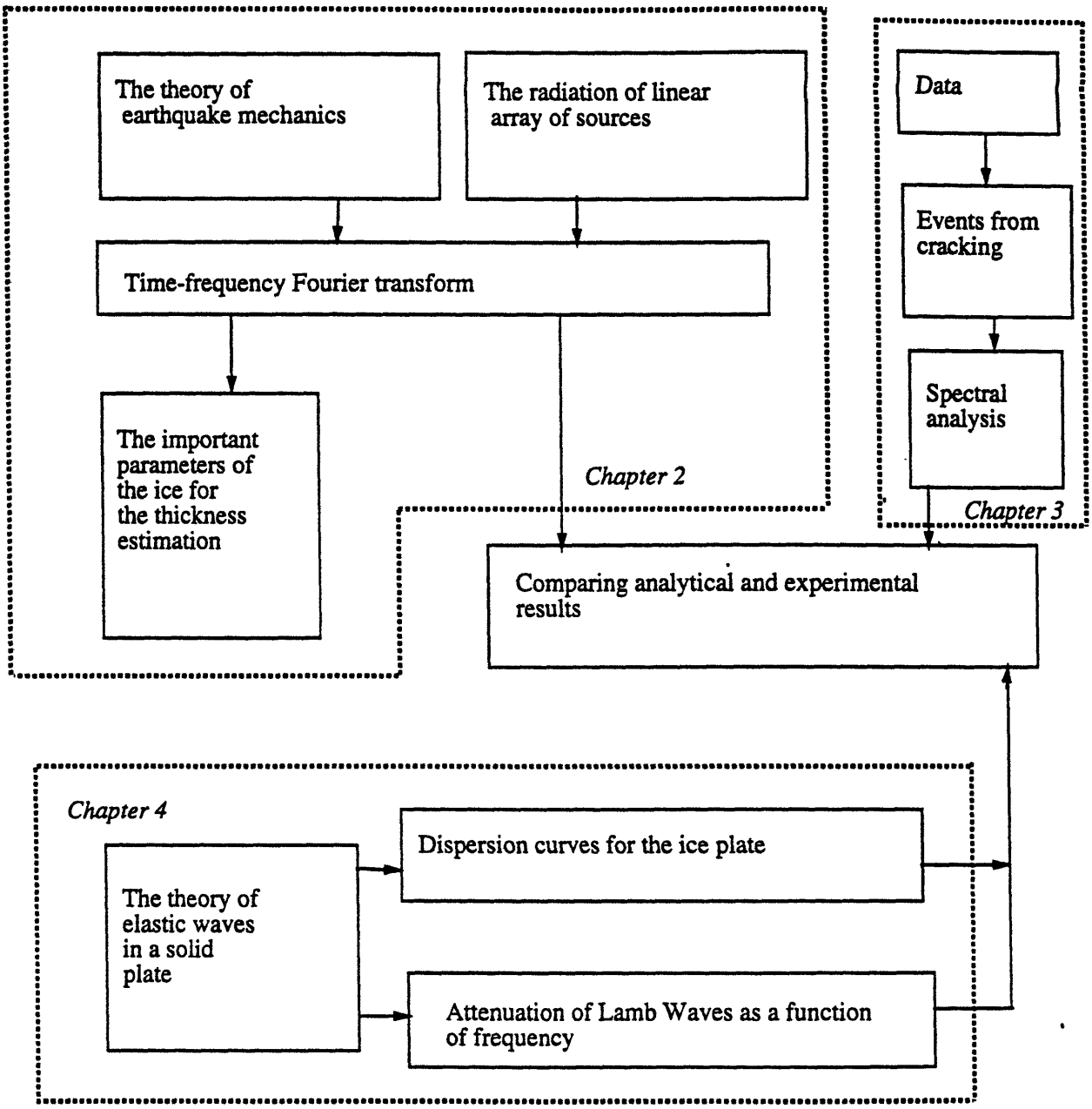

Figure 1-2: The approach for the estimation of ice thickness from ambient noise

Chapter 2

Analytical Model for the Propagating Ice Cracks

In this chapter the theoretical relationship between ice thickness and the direct acoustic signal from the crack is considered. (The waves that propagate in the ice sheet and their influence on the detected under-ice signal is considered in Chapter 4.)

First, the "moving" effect in the crack formation is considered by representing a propagating crack like a linear array of sources.

Second, similar to earthquake mechanics, a sinusoidally roughened ramp function is introduced to represent the displacement of the fault planes. This function is a key point in the relationship between the ice thickness and the sound waves from a crack.

Then, previous results are summarized to identify some properties of the spectral density function of the signal at the point of the receiver. Numerical examples for some cases of the crack and receiver positions, as well as crack and ice parameters, are also shown.

2.1 Propagating crack like a linear array of sources.

The theoretical simulation of an under-ice signal from a propagating crack like the radiation from a linear array of sources is considered in this section.

Cracks occurring in the ice can range in length from few meters to kilometers,

but all of them roughly follow a rule: they are lines or consist of linear segments. Therefore, the fault surface can be modeled as linear array of discretized sound sources (see Fig. 2.1). The total pressure at the point of receiver, which is placed in the ocean under the ice plate, can be expressed as:

$$p(x,t) = p_{left} + p_{right}, \tag{2.1}$$

where p_{left} is the pressure field from the left side of an array (or crack) and p_{right} is the pressure field from the right.

In the beginning, assume an array of discretized sources for simplicity:

$$p_{right} = \frac{A}{L}\frac{\Delta l}{r}[w(t-\frac{r}{c}) + w(t-\frac{r-\Delta\tilde{l}}{c}-\frac{\Delta l}{v}) + w(t-\frac{r-2\,\Delta\,\tilde{l}}{c}-\frac{2\,\Delta\,l}{v}) + ...], \tag{2.2}$$

where $w_i(t) = w(t)$ is the source function of the i-th discrete source
(assumed identical for all sources),

L is the crack length,

A is the source strength of an array,

v is the crack propagating speed,

Δl is the linear distance between the discretized sources,

$\Delta\tilde{l}$ is the apparent distance between adjacent discrete sources to the receiver,

r is the distance between the center of the crack and the point of the receiver,

c is the sound speed in water (assumed constant).

The distance between the adjacent discretized sources to the receiver may be obtained by geometry (see Fig. 2.1):

$$\Delta\,\tilde{l} = \Delta l sin\gamma cos(\theta - \theta_r), \tag{2.3}$$

where γ is the angle between axis z and r,

θ is the angle between axis x and crack-direction,

θ_r is the angle between axis x and the projection of r onto (xy) surface

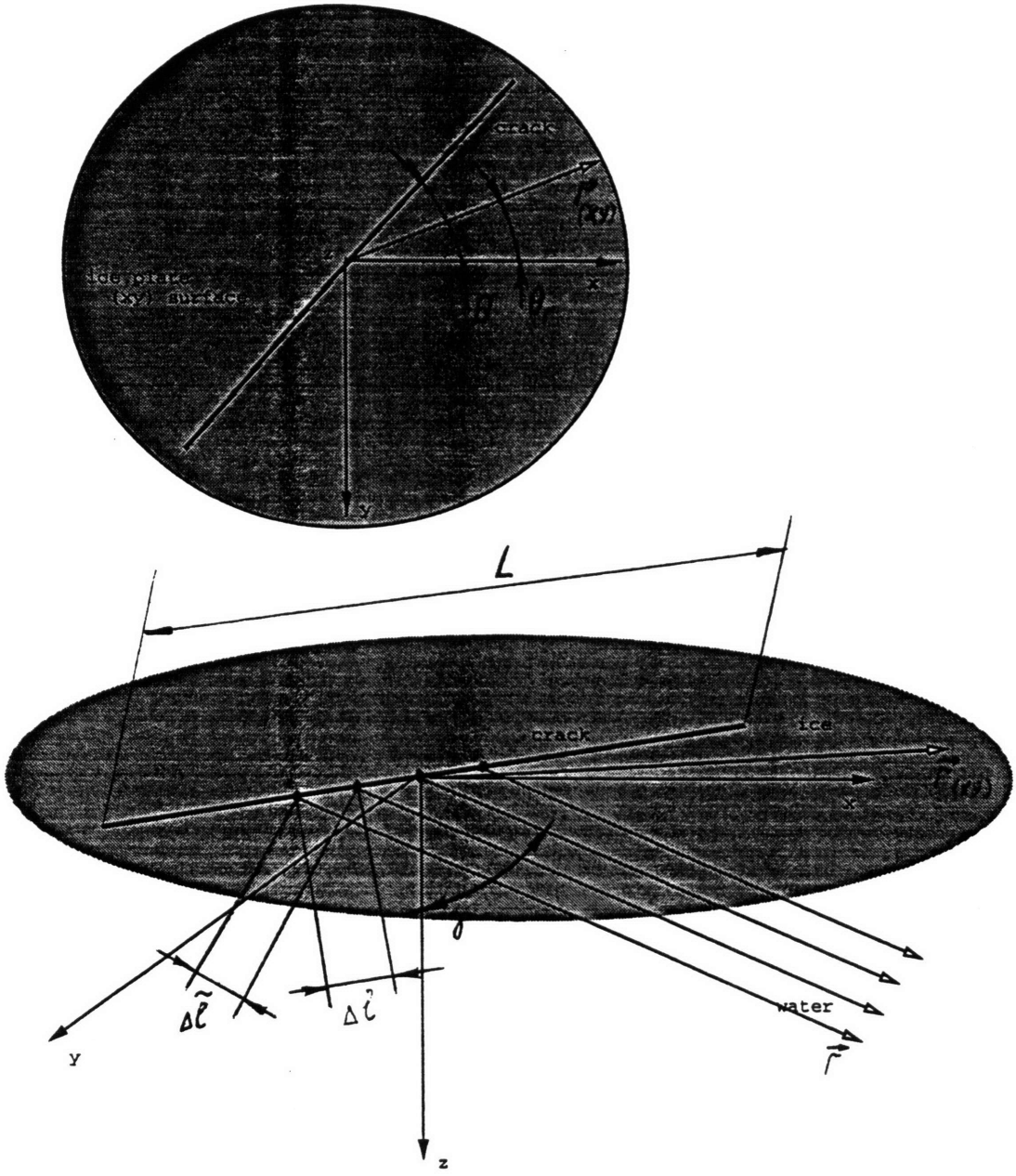

Figure 2-1: Propagating crack and coordinate system

Equation (2.2) may be rewritten:

$$p_{right}(x,t) = \frac{A}{L}\frac{\Delta l}{r}\sum_{n=0}^{N} w(t - \frac{r}{c} + \frac{n\Delta\tilde{l}}{c} - \frac{n\Delta l}{v}). \tag{2.4}$$

For the limited case of $\Delta l \to 0$, that is for the continuously distributed sources, the expression (2.4) reduces to integral form

$$p_{right}(x,t) = \frac{A}{L}\frac{1}{r}\int_0^{L/2} w(t - l(\frac{1}{v} - \frac{sin\gamma cos(\theta-\theta_r)}{c}) - \frac{r}{c})dl = \frac{A}{L}\frac{1}{r}\int_0^{L/2} w(t - \frac{r}{c} - lk_1)dl, \tag{2.5}$$

where

$$k_1 = \frac{1}{v} - \frac{sin\gamma cos(\theta-\theta_r)}{c}. \tag{2.6}$$

In a similar way, we reduce the left side of array:

$$p_{left}(x,t) = \frac{A}{L}\frac{1}{r}\int_{-L/2}^{0} w(t - \frac{r}{c} - lk_2)dl, \tag{2.7}$$

where

$$k_2 = -\frac{1}{v} - \frac{sin\gamma cos(\theta-\theta_r)}{c}. \tag{2.8}$$

Using the transformation $k_1 l = \tau_1$ in (2.7)

$$p_{right}(x,t) = \frac{A}{L}\frac{1}{r}\frac{1}{k_1}\int_0^{k_1 L/2} w(t - \frac{r}{c} - \tau_1)d\tau_1 = \frac{A}{Lrk_1}\int_{-\infty}^{\infty} w(t - \frac{r}{c} - \tau_1)g_1(\tau_1)d\tau_1, \tag{2.9}$$

where

$$g_1(\tau_1) = \begin{cases} 0, & \tau_1 < 0 \\ 1, & 0 < \tau_1 < k_1 L/2 \\ 0, & \tau_1 > k_1 L/2 \end{cases}. \tag{2.10}$$

By the definition of the convolution of the two functions, the expression (2.9) may be rewritten:

$$p_{right}(x,t) = \frac{A}{Lr} w(t - \frac{r}{c}) * \frac{1}{k_1} g_1(t). \tag{2.11}$$

In the same way, for the left side of the crack,

$$p_{left}(x,t) = -\frac{A}{Lrk_2}\int_{-\infty}^{\infty} w(t-\frac{r}{c}-\tau_2)g_2(\tau_2)d\tau_2 = -\frac{A}{Lr}w(t-\frac{r}{c}) * \frac{1}{k_2}g_2(t), \quad (2.12)$$

where

$$g_2(\tau_2) = \begin{cases} 0, & \tau_2 < 0 \\ 1, & 0 < \tau_2 < -k_2L/2. \\ 0, & \tau_2 > -k_2L/2 \end{cases} \quad (2.13)$$

Note that k_2 is negative.

The total pressure field can be calculated with the help of expression (2.9) for p_{right} and (2.12) for p_{left} and (2.1) :

$$p(x,t) = -\frac{A}{Lr}w(t-\frac{r}{c}) * (\frac{1}{k_1}g_1(t) - \frac{1}{k_2}g_2(t)). \quad (2.14)$$

So the pressure field is the convolution of two functions. The sum of two rectangular boxes is the result of uniform source strength distribution along the crack surface using a farfield approximation. In reality, the source strength function does not have to be a box type; it can be triangle, or any kind of shape that best describes the source strength distribution. The rectangular shape will be assumed for simplicity.

2.2 The displacement at the point of cracking

Several models for the elemental source function $w(t)$ were suggested in previous studies. In Ref. [5] the elemental crack is modeled by an approximate "equivalent source," and the example chosen represents a small failure of the ice sheet under tension. The interesting models proposed in Ref. [6], where a crack in the ice plate is described as a combination of seismic sources, and analytical solutions are developed for tensile crack, dip-slip and strike-slip. In Ref. [4] a detailed numerical investigation of Ewing and Press's characteristic equation for the case of a monopole source is carried out. In [6] the impulse source function is assumed.

As a compliment to these theoretical efforts, the model described below is based

on a more realistic assumption to obtain the information about the ice sheet. Observations of cracking events [9],[10] show some similarities to seismic signals, and this has motivated the approach to the analysis of the ice sheet in which a theory of earthquake mechanics is used.

By analogy with earthquake theory [11], the fault displacement-time function should be choosen for the model of an elemental source . The most realistic representation for the displacement function at the point of cracking is a somewhat roughened ramp function. As an approximation to such a function a ramp modulated by a sine wave is considered:

$$G(t) = \begin{cases} 0 & t < 0 \\ \frac{1}{T}(t + \frac{T}{2n\pi}\sin\frac{2n\pi t}{T}) & 0 < t < T, \\ 1 & t > 0 \end{cases} \tag{2.15}$$

where T is the rise time,

n is the integer equal to the number of rougheness elements in the fault (assume $n = 1$ for the ice plate).

I follow Ref. [9] and take the roughness elements to be some fraction ϵ of the primary amplitude. The normalized fault displacement is modeled as

$$G(t) = \begin{cases} 0 & t < 0. \\ \frac{1}{T}(t + \epsilon\frac{T}{2n\pi}\sin\frac{2n\pi t}{T}) & 0 < t < T. \\ 1 & t > 0 \end{cases} \tag{2.16}$$

The corresponding displacement velocity would be

$$U(t) = G'(t) = \begin{cases} 0 & t < 0 \\ \frac{1}{T}(1 + \epsilon\cos\frac{2n\pi t}{T}) & 0 < t < T. \\ 0 & t > 0 \end{cases} \tag{2.17}$$

The physical concept here is of a "slip-stick" shear-fault, or of a tensile fault where the yeild point advances in small jumps determined by the thickness of the

ice sheet. The slip or tear on the fault is controlled by the narrowest dimension of rupture surface, which for large cracks, fracturing the ice over its full depth, is *the ice thickness.*

In earthguake mechanics [12], it is generally assumed that at any given point the crack continues to widen until the rupture front is $h/2$ past that point, where h is the ice thickness. Using this assumption here, the rise time is

$$T = \frac{h}{2v}, \tag{2.18}$$

where v is the rupture velocity.

The elemental crack source function is

$$Q = \int_S U(t)dS = 2AU(t), \tag{2.19}$$

where $U(t)$ is the velocity at the point of cracking,

A is the area of the fault plane per unit length. ($A = h$, numerically.)

After plugging (2.17) into (2.19)

$$w(t) = Q(t) = 2h \begin{cases} 0 & t < 0 \\ \frac{1}{T}(1 + \epsilon \cos \frac{2n\pi t}{T}) & 0 < t < T. \\ 0 & t > 0 \end{cases} \tag{2.20}$$

The shape of this function in the time domain is shown in Fig. 2.3a.

2.3 PSD of the water-born acoustic signal

Summarizing the analytical results for the model of the propagating crack as the linear array of moving sources (Section 2.1) and for the source function as the volume change at the point of cracking for the source function (Section 2.2), the

pressure field in the water is

$$p(x,t) = -\frac{A}{Lr} w(t - \frac{r}{c}) * (\frac{1}{k_1} g_1(t) - \frac{1}{k_2} g_2(t)), \tag{2.21}$$

where

$$g_1(t) = \begin{cases} 0, & t < 0 \\ 1, & 0 < t < k_1 L/2, \\ 0, & t > k_1 L/2 \end{cases} \tag{2.22}$$

$$g_2(t) = \begin{cases} 0, & t < 0 \\ 1, & 0 < t < -k_2 L/2, \\ 0, & t > -k_2 L/2 \end{cases} \tag{2.23}$$

$$w(t) = 2h \begin{cases} 0 & t < 0 \\ \frac{1}{T}(1 + \epsilon \cos \frac{2n\pi t}{T}) & 0 < t < T, \\ 0 & t > 0 \end{cases} \tag{2.24}$$

where k_1 and k_2 are some constants(see eqns. (2.6) and (2.8) dependent on the positions of the crack and the point of the receiver.

Since the convolution in the time domain corresponds to the multiplication of two Fourier transforms in the frequency domain, it is useful to look at the frequency domain solution.

The Fourier transform of

$$f_1(t) = \frac{1}{k_1} g_1(t) - \frac{1}{k_2} g_2 \tag{2.25}$$

is

$$F_1(f) = \frac{1}{k_1} F_{11}(f) - \frac{1}{k_2} F_{12}(f), \tag{2.26}$$

where $F_{11}(f)$ and $F_{12}(f)$ are Fourier transforms from rectangular boxes:

$$F_{11}(f) = \int_{-\infty}^{\infty} g_1(t)^{i2\pi ft} dt = \exp(i\pi f k_1 L/2) k_1 L/2 sinc(\pi f k_1 L/2), \tag{2.27}$$

and

$$F_{12}(f) = \int_{-\infty}^{\infty} g_2(t)^{i2\pi ft} dt = -\exp(-i\pi f k_2 L/2) k_2 L/2 sinc(\pi f k_2 L/2). \qquad (2.28)$$

Fig. 2.2a shows the functions $\frac{1}{k_1} g_1(t)$ and $\frac{1}{k_2} g_2(t)$ in the time domain. Fig. 2.2b shows the power spectral density (PSD) of $f_1(t)$ or $|F_1|^2$.

The Fourier transform of $f_2(t) = w(t)$ is the summation of the Fourier transform of the rectangular box and the rectangular box multiplied on the *cosine* function. Using the cosine modulation rule:

$$T(u) cos 2\pi a u \longrightarrow \frac{1}{2} B(s-a) + \frac{1}{2} B(s+a) \qquad (2.29)$$

(where u is a time variable, s is a frequency variable, and $T(u) \longrightarrow B(s)$) the Fourier transform of $f_2(t) = w(t)$ is

$$F_2(f) = \int_{-\infty}^{\infty} f_2(t) exp(i2\pi ft) dt, \qquad (2.30)$$

or

$$\begin{aligned} F_2(f) \quad &= 2h(e^{i\pi fT} sinc(\pi fT) \\ &+ \tfrac{T\epsilon}{2}(e^{i\pi(f-\frac{1}{T})T} sinc(\pi(f-\tfrac{1}{T})T) \\ &+ e^{i\pi(f+\frac{1}{T})T} sinc(\pi(f+\tfrac{1}{T})T)). \end{aligned}$$

Fig. 2.3 shows $f_2(t)$ in the time domain and the power spectral density $|F_2|^2$. The total power spectral density of the signal $p(x,t)$ (Eq.(2.21)), is

$$F(f) = F_1(f) \cdot F_2(f). \qquad (2.31)$$

The spectrum of the water-born acoustic signal at the point of the receiver for different cases of ice thickness, crack length, and position of the receiver is discussed in the next section.

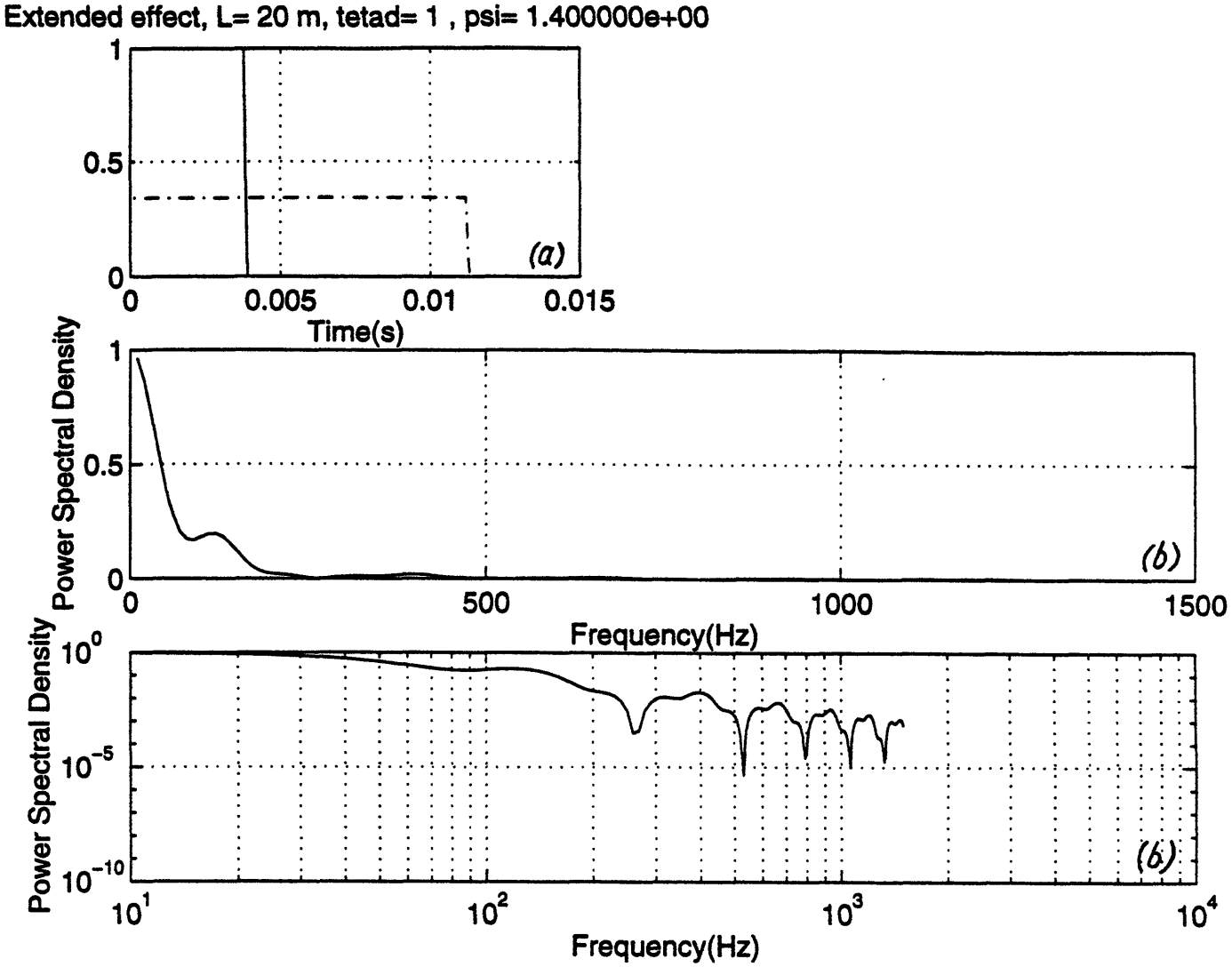

Figure 2-2: The shape of $f_1(t)$ *(a)* in the time domain and *(b)* in frequency domain for the crack with length 20 m, $\theta = 0$ rad, $\theta_r = 1$ rad and $\gamma = 1.4$ rad.

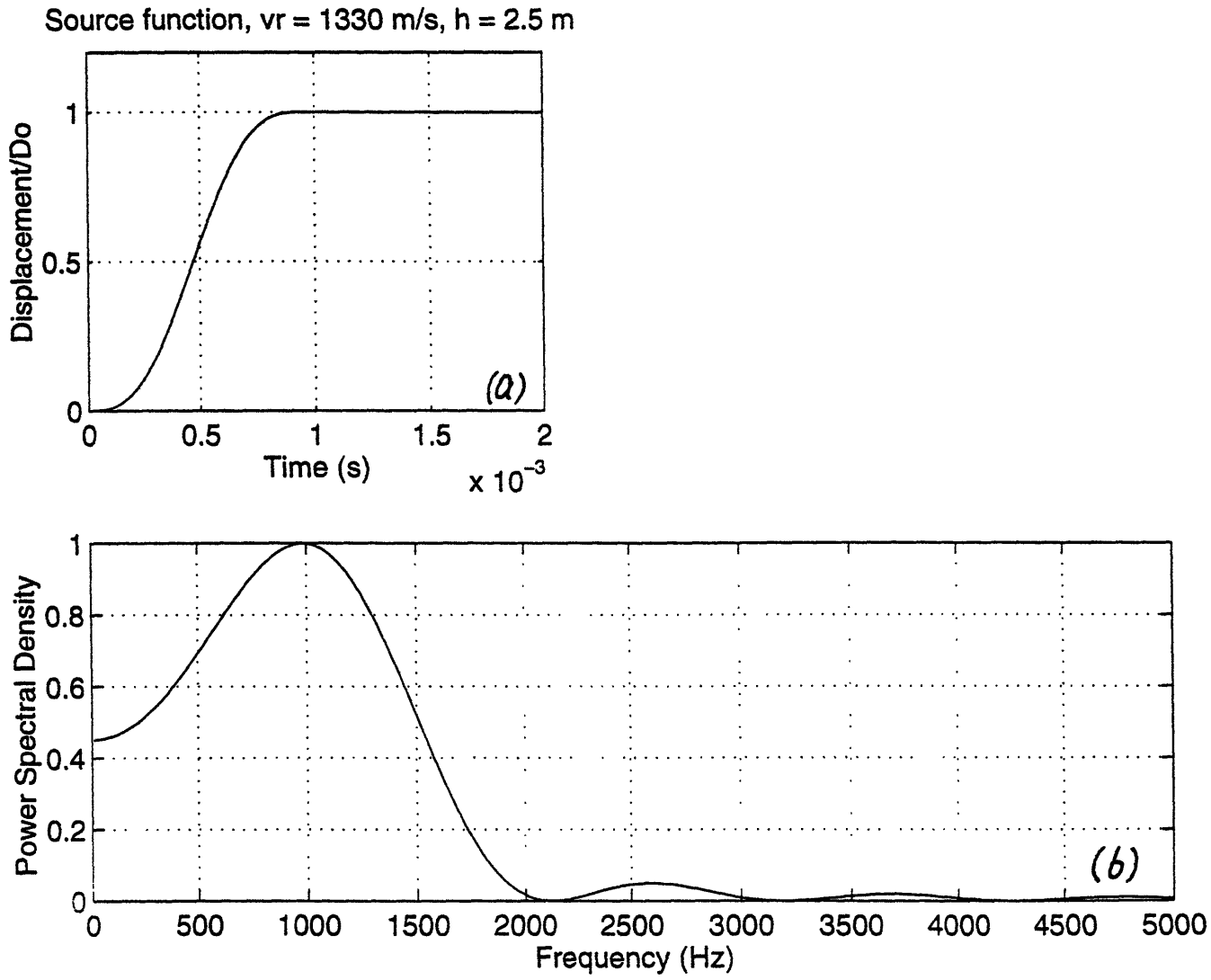

Figure 2-3: The shape of $f_2(t)$ *(a)* in the time domain and *(b)* in the frequency domain for ice thickness of 2.5 m and v,crack propagating speed, = 1330 m/s

2.4 Analytical results for different cases

In this section, the acoustic emission from a propagating crack in the ice plate is studied using the developed analytical model developed in the previous section. The sound speed in the water is assumed to be 1440 m/s. The rupture speed is 1330 m/s. (See the next section)

The following parameters of the *ice* are important for the shape of the signal from the crack (Expression 3.1 of previous section)

- h - the ice thickness,
- v - the rupture velocity (See Section 2.5.).

The following parameter of the *crack* are important for the shape of (2.31):

- L - the crack length.

The *position* of the crack with respect to the point of the receiver also determines the shape of the signal. The position is described by

- γ, the angle between axis z and direxction r,
- θ, the angle between axis x and the crack-direction,
- θ_r, the angle between axis x and the projection of r onto (xy) surface, and
- r, the distance between the center of the crack and the receiver point.

The goal of the analytical solutions is to understand the relationship between these parameters and the spectral power density of the signal.

Case 1. *Different crack lengths:* The results are shown in Fig. 2.4 for the power spectral density of the water-born acoustic signal in the point of receiver. The ice thickness, the rupture velocity, the crack and receiver positions are the same for all four curves.

Case 2. *Different receiver locations:* The power spectral dencity curves for different values of the angle between axis z (see Fig. 2.1) and direction to the receiver $\vec{r}$ are

shown in Fig. 2.5. The ice thickness, the rupture velocity, the crack length and position in the ice plate are the same for all four curves.

Case 3. *Different crack positions on the ice plate:* (rotating around the crack center) The results of numerical calculations of the power spectral density of the water-born acoustic signal are shown in Fig. 2.6. The ice thickness, the rupture velocity, the crack length and the position of the hydrophone in the ocean are the same for all four curves.

Case 4. (the most important) *Different ice thicknesses:* To show the relationship between ice thickness and the position of the peak in the graph for the power spectral density function for the acoustic signal from the propagating crack is the goal of Fig. 2.7. For all curves the position of the receiver in the ocean and the crack in the ice plate are the same.

Summarizing the results of these four cases we can conclude that the frequency with which the peak occurs on a power spectral density curve is defined mostly by the value of the ice thickness.

2.5 The rupture speed of the Arctic Ice

What is important to know about Arctic ice for estimating the ice thickness by this analytical approach? According to the analytical model, the important feature is the peak in the power spectral density function of the water-born signal from a propagating crack penetrating the ice over its full depth. Assume that this peak is f_0. Using (1.18) we can calculate

$$h = \frac{2v_r}{f_0}, \tag{2.32}$$

where v_r is the rupture speed in the ice.

In this step, the most important parameter for discussion is the rupture speed for the Arctic ice.

According to [10], in fracture mechanics v_r is variously taken to be $v_r < c_r$, with c_r as the Rayleigh wave speed; or $0.8c_s$, with c_s as the shear speed; or $0.38c_p$, with c_p as the compressional speed [13],[14]. For sea ice, $c_r \approx 1700$ m/s, $c_s \approx 1800$ m/s,

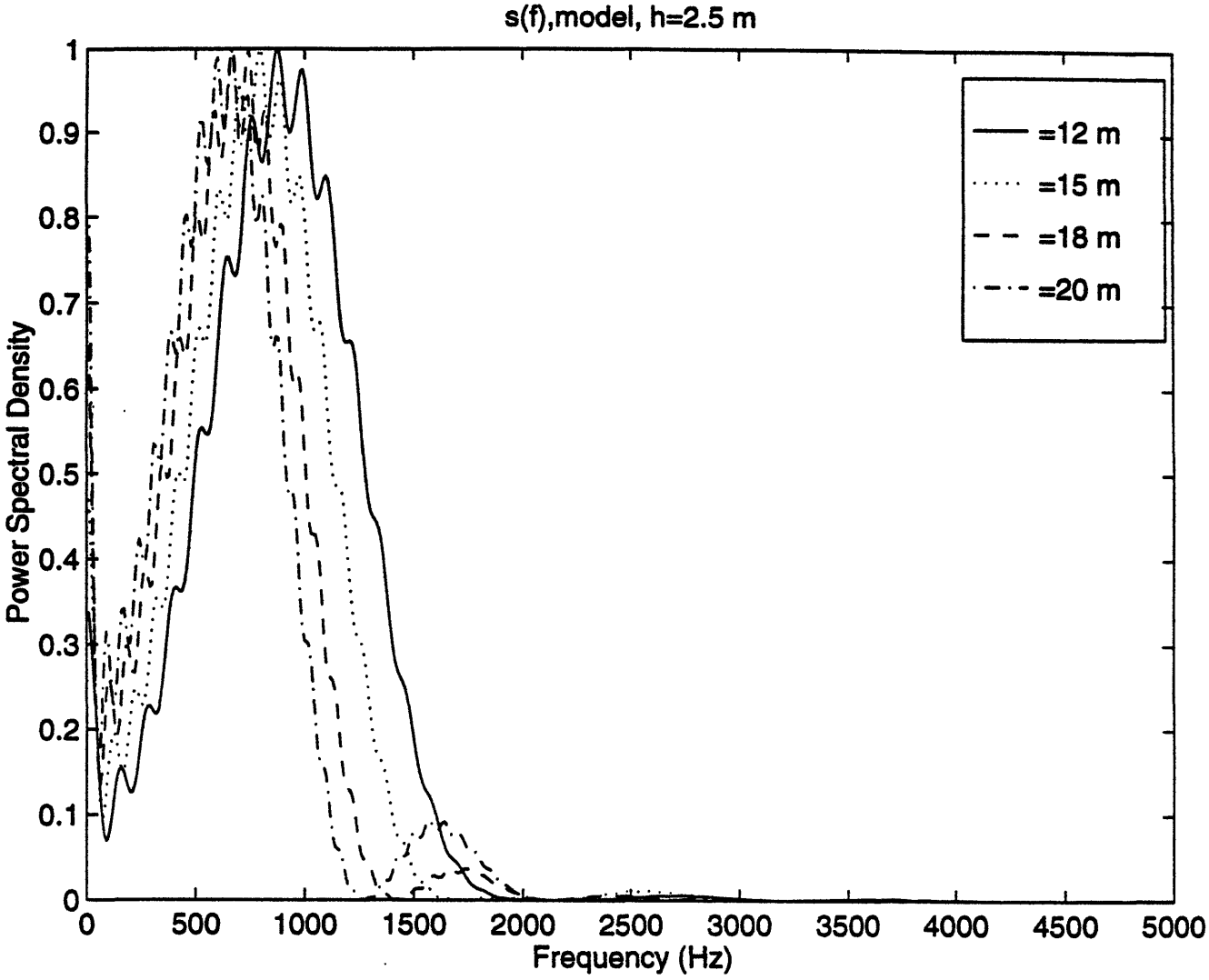

Figure 2-4: Analytical result: The power spectral density $|F(f)|^2$ for the propagating crack with $c = 1440$ m/s; $v = 1330$ m/s; $r = 500$ m; $h = 2.5$ m; $\gamma = 80°$; $\theta = 10°$; $L = 12, 15, 18, 20$ m.

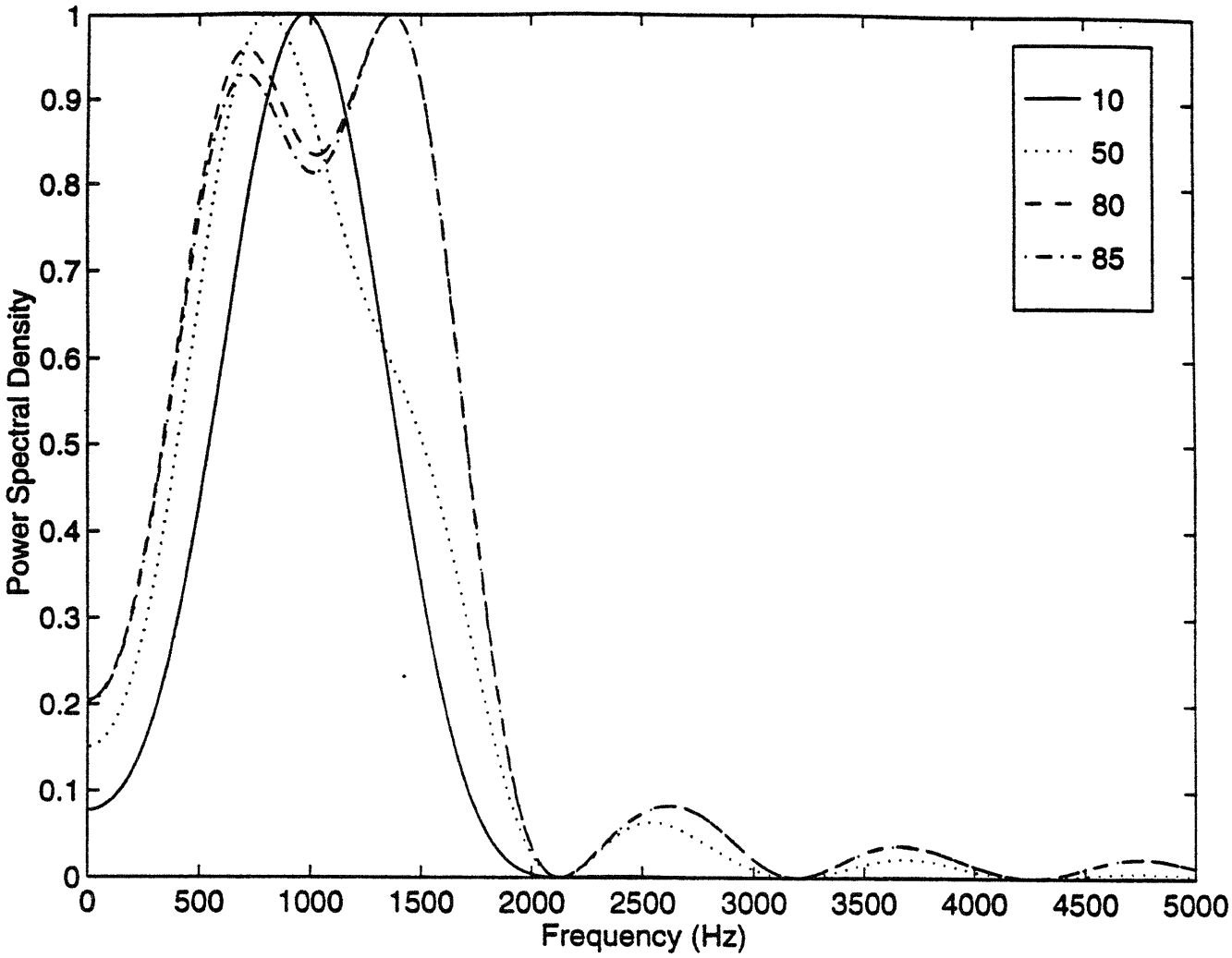

Figure 2-5: Analytical result: The power spectral density $|F(f)|^2$ for the propagating crack with $c = 1440$ m/s; $v = 1330$ m/s; $r = 500$ m; $L = 1$ m; $h = 2.5$ m; $\theta = 0°$; $\gamma = 10°, 50°, 80°, 85°$.

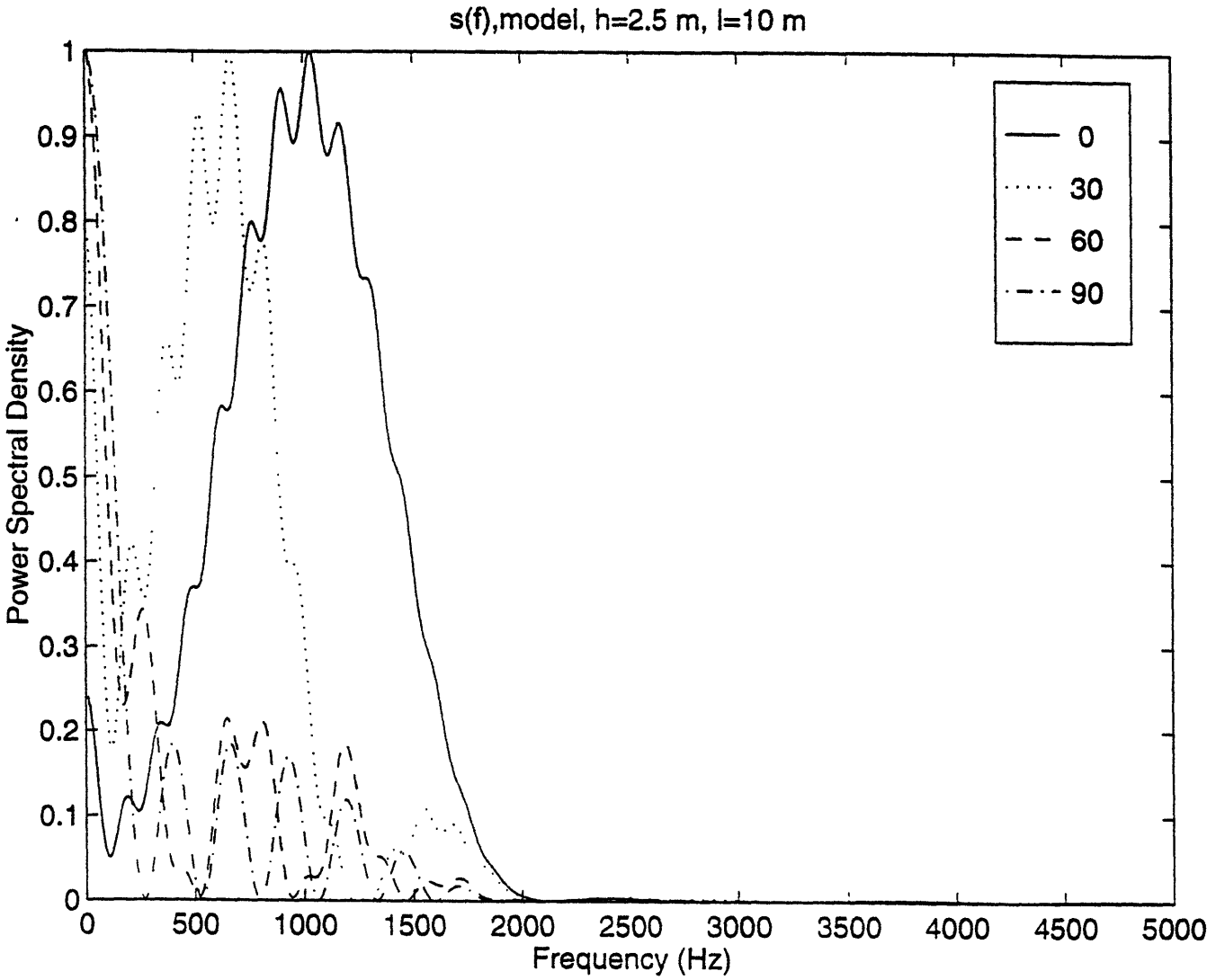

Figure 2-6: Analytical result: The power spectral density $|F(f)|^2$ for the propagating crack with $c = 1440$ m/s; $v = 1330$ m/s; $r = 500$ m; $L = 10$ m; $h = 2.5$ m; $\gamma = 80^o$; $\theta = 0^o, 30^o, 60^o, 90^o$.

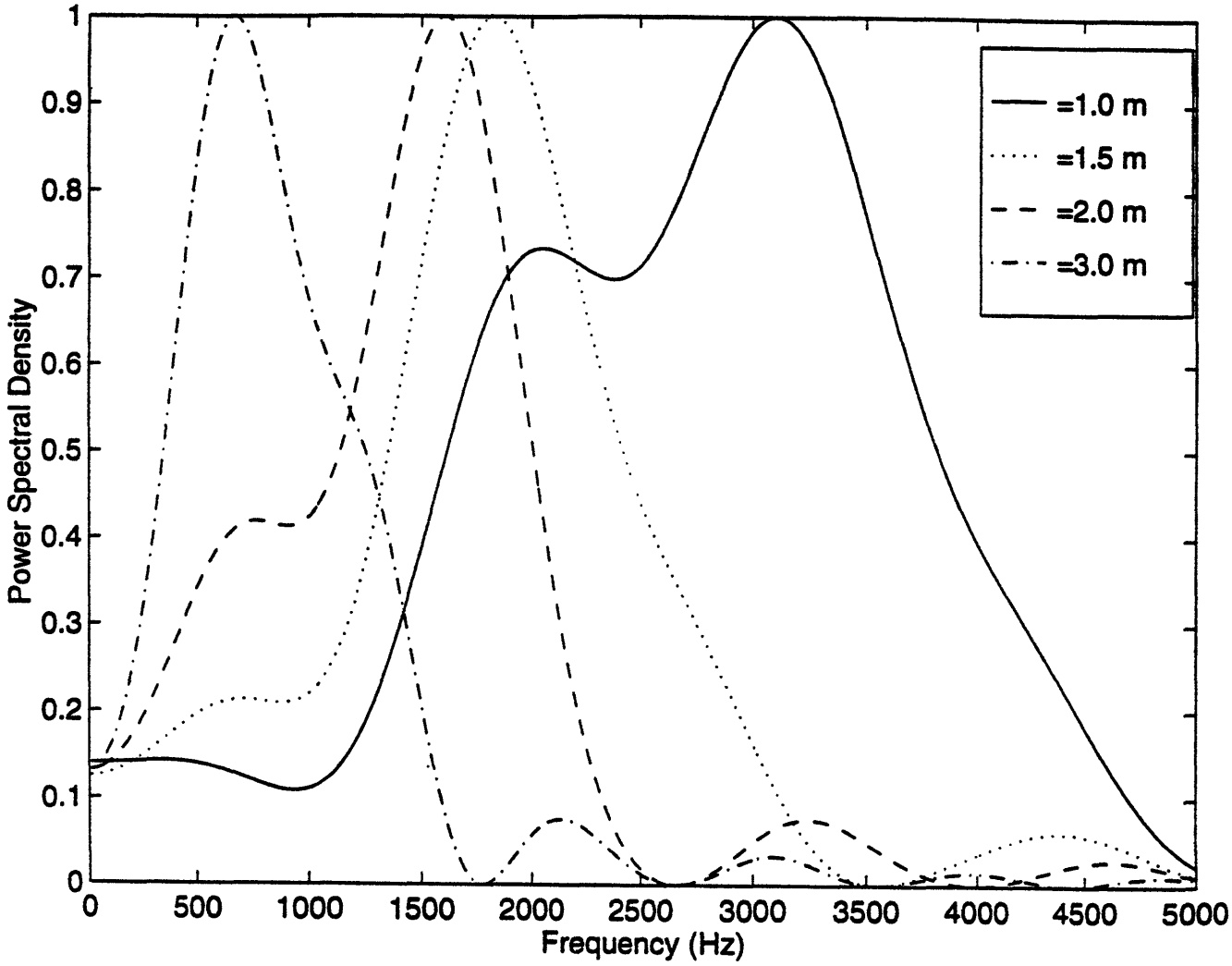

Figure 2-7: Analytical result: The power spectral density $|F(f)|^2$ for the propagating crack with $c = 1440$ m/s; $v = 1330$ m/s; $r = 500$ m; $L = 1$ m; $\gamma = 80^o$; $\theta = 0^o$; $h = 1.0, 1.5, 2.0, 3.0$ m.

h (m)	c_p (m/s)	c_s (m/s)
1.18	3000	1590
2.40, 2.37, 2.15	3500	1750

Table 2.1: Best compressional/shear speeds and ice thicknesses determined by 1987 PRUDEX

and $c_p \approx 3500$ m/s (See Ref.4). [10] used v_r=1440 m/s, a value within 15% of the various estimates.

In Ref.15 different values for the rupture speed are presented. v_r (max) $\approx 0.63 c_s$ for Poisson's ratio $\sigma = 0.25$. Therefore, v_r (max) $\approx 0.63 \cdot 1800 = 1134$ m/s.

For the value of shear speed the data are different, too. In [4] $c_s = 1800$m/s, but in [16] $c_s = 1900$m/s.

In [17] the value of bulk compressional and shear speeds obtained for the thicker multi-year ice at the PRUDEX ice camp, 3500m/s and 1750m/s, respectively, compare very well with similar values obtained by earlier investigators. Note, also, that the shear speed measured in the annual ice, 1590 m/s is considerably lower, older than in the thicker ice (See Table 2.1).

Analyzing previous estimates, I use v_r=1330m/s for rupture speed in the ice.

Chapter 3

The analysis of experimental data

The hydrophone data analyzing in this chapter were recorded in the Beaufort Sea during the Spring 1994 MIT Arctic expedition; 86 crack signals were chosen for analysis.

The Maximum Likelihood (Capon) Spectral Estimation is used because the signals from cracks are short in time.

In the section 3.3 a histogram for all 86 events is provided. The method of ice thickness estimation from analysis of the real hydrophone data is shown using the histogram.

Some properties common to all recorded signals properties other than the spectral peak near 1 kHz are noted. The hypothesis is that some other sound waves, not only direct-acoustic waves, contribute to the analyzed hydrophone signals.

3.1 Instrumentation and recorded data

The deployment consisted of one a broadband recording acoustic hydrophone. The camp location of the MIT expedition camp was 149 degrees 33 minutes west and 73 degrees 0 minutes north. (See Fig. 3.1.) Fig 3.2. shows the deployment place of the hydrophone. The recording time is 20 seconds. Data was recorded on a DAT tape sampled at 32 kHz (20 Hz to 14.5 kHz useful bandwidth), then subsequently redigitized on a Macintosh at 22 kHz. Since the theoretical approach requires the

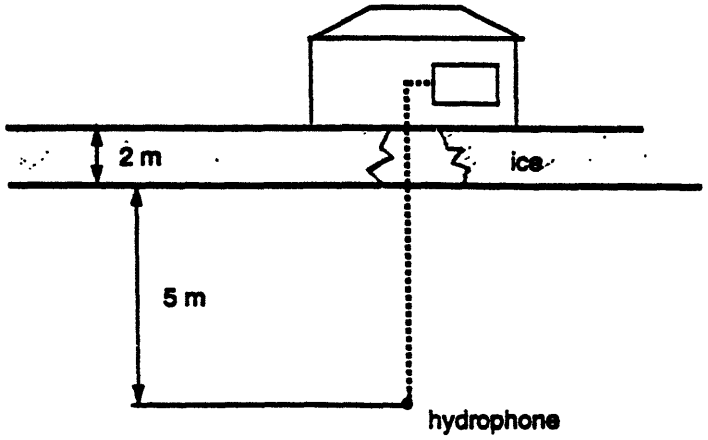

Figure 3-1: Chart of the MIT camp showing the hydrophone deployment

accuracy on high frequencies the large bandwidth (more than 10 kHz) hydrophone was used for measurements. The data is discretely sampled with $\Delta t = 4.4934 \cdot 10^{-5}$ s.

During the recording time some fracturing occured in the region. The data looks like noise with many higher amplitude events, approximately 20 ms in length. (See Fig. 3.3) It is not easy to determine from the observation of the events, which ones are from cracks and which are from another sources. For analysis 86 events were chosen that show some similarities by shape with each other and with seismic signals. The typical event is shown in Fig. 3.4.

3.2 The method of spectral analysis

Estimation of the power spectral density (PSD), or simply the spectrum, of discretely sampled deterministic and stochastic processes is usually based on the fast Fourier transform (FFT). This approach to spectrum analysis is computationally efficient and produces reasonable results for a large class of signal processes. But Kay and Marple note in [18], that in spite of these advantages, there are several inherent per-

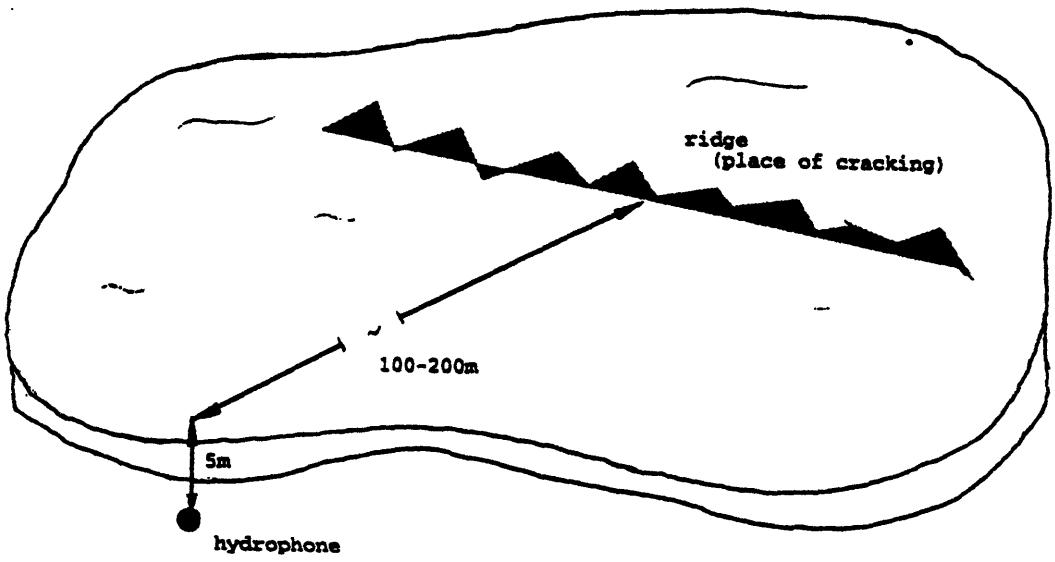

Figure 3-2: Chart showing the place of cracking in the ice and the hydrophone deployment in the ocean

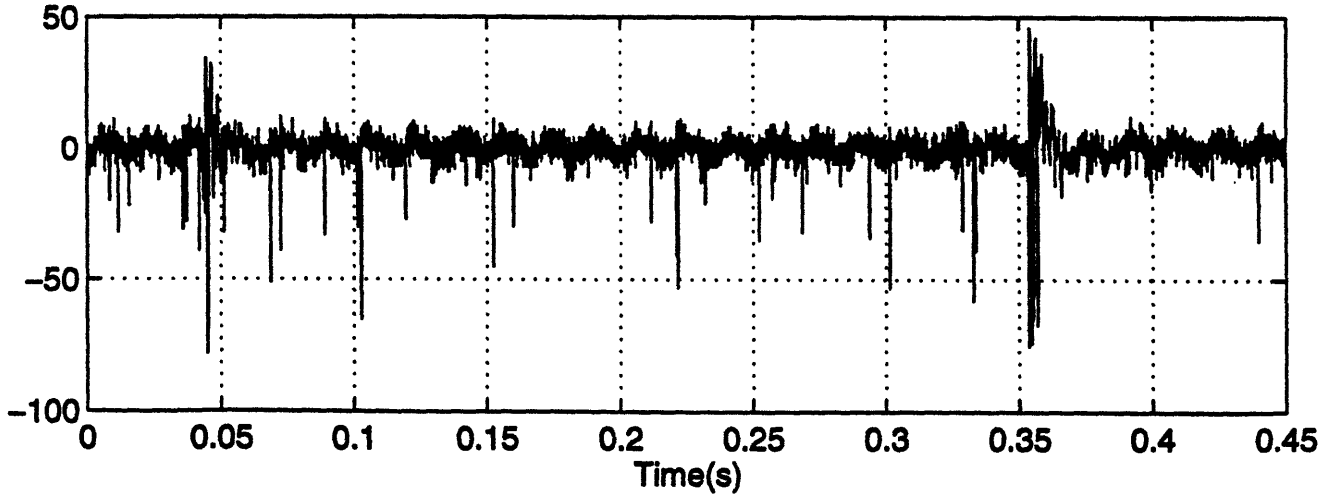

Figure 3-3: Sound-pressure time plot for ice noise with crack-events.

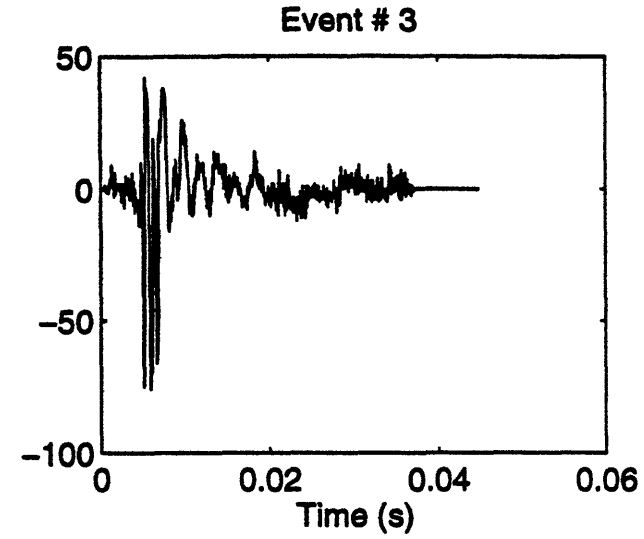

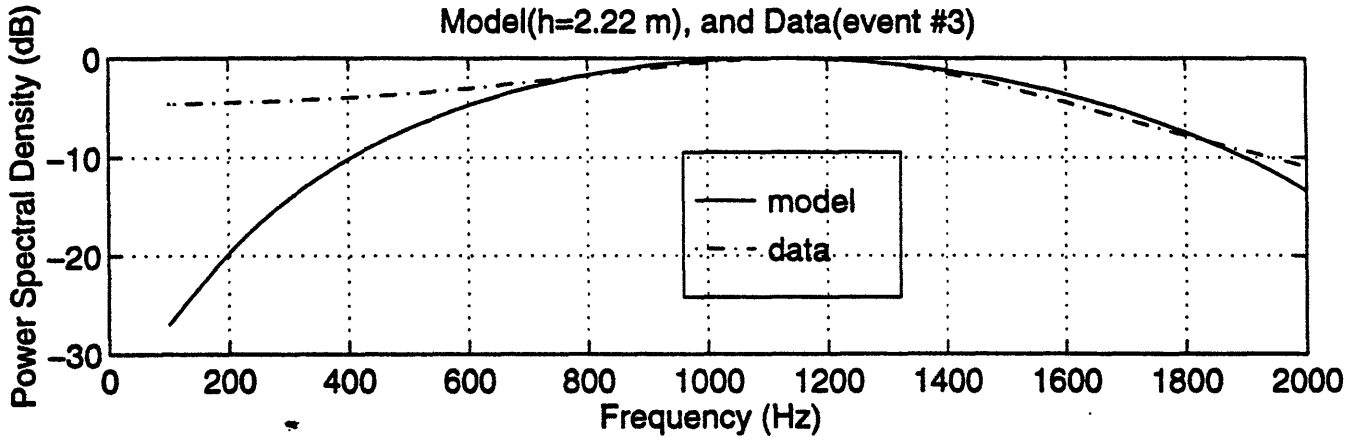

Figure 3-4: The event #3 in the time domain, and power spectral density in frequency domain for the first part of the signal, and simulation of the spectrum of the direct propagating wave from a crack for h=2.22 m.

formance limitations of the FFT, such as frequency resolution and implicit windowing of the data. These two performance limitations of the FFT method are particularly troublesome when analyzing short data records, the situation which we have with crack signals.

The signals of interest in this research have a temporal duration of approximately 15-20 ms. The maximum likelihood spectral estimation (MLM) is used for crack data analysis in this research. MLM was originally developed for seismic array frequency-wave number analysis. The approach uses the following theoretical considerations.

In MLM one estimates the PSD by effectively measuring the power out of a set of narrow-band filters. The shape of these filters (See Ref. [18]) are different for each frequency; they are finite impulse response types with p weights (taps),

$$A = [a_0 a_1 ... a_{p-1}]^T. \tag{3.1}$$

The coefficients are chosen so that at the frequency under consideration, say f_0, the frequency response of the filter is unity (i.e., an input sinusoid at that frequency would be undistorted at the filter output) and the variance of the output process is minimized. Thus the filter should adjust itself to reject components of the spectrum not near f_0 so that the output power is due mainly to frequency components close to f_0. To obtain the filter, one minimizes the output variance σ^2, given by

$$\sigma^2 = [A]^H [R_{xx}][A] \tag{3.2}$$

subject to the unity frequency response constraint (so that the sinusoid of frequency f_0 is filtered without distortion),

$$[E]^H [A] = 1, \tag{3.3}$$

where $[R_{xx}]$ is the covariance matrix of x_n, E is the "steering" vector

$$E = [\exp(j2\pi f_0 \Delta t) \ \exp(j2\pi 2 f_0 \Delta t) \ ... \exp(j2\pi(p-1) f_0 \Delta t)]^T, \tag{3.4}$$

and H denotes the complex conjugate transpose. The solution for the filter weights is

$$A_{opt} = \frac{[R]_{xx}^{-1}[E]}{[E]^H[R]_{xx}^{-1}[E]}, \tag{3.5}$$

and the minimum output variance is then

$$\sigma_{min}^2 = \frac{1}{[E]^H[R_{xx}]^{-1}[E]}. \tag{3.6}$$

It is seen that the frequency response of the optimum filter is unity at $f = f_0$, and that the filter characteristics change as a function of the autocorrelation function. Since the minimum output variance is due to frequency components near f_0, then $\sigma_{min}^2 \Delta t$ can be interpreted as a PSD estimate. Thus, the MLM power spectral density is defined as

$$S(f_0) = \frac{\Delta t}{[E]^H[R_{xx}]^{-1}[E]}. \tag{3.7}$$

To compute the spectral estimate, one only needs an estimate of the autocorrelation matrix.

The disadvantage of MLM estimate are that is a smooth spectrum (it cannot resolve the two closely spaced sinusoidal components), and the estimation is non-linear (amplitudes are not preserved). But it is not important in terms of the ice thickness determination from the signals from cracks.

3.3 Typical results for a signal from a crack

The MLM estimate as a function of frequency for the event # 3 is shown in Fig. 3.4. The first 3 ms of the event is analyzed. The correlation matrix is developed for 25 time points. For the comparing with the theoretical model the curve for $h = 2.22m$ is on the same plot. One can see the peak near 1000 Hz. From direct measurements of ice thickness at the site (near ridge) it is known that ice is approximately 2.5 m thick . Thus one can predict an expected peak in the frequency domain by theoretical

approach:

$$f = \frac{2v}{h} = \frac{2 \cdot 1330}{2.5} = 1064(Hz) \tag{3.8}$$

This value is consistent with the experimental data.

3.4 Some statistics for 86 events

In previous section it is noted that the peak in the spectral estimate of the first part of the event # 3 is consistent with the theoretical prediction. Then, consider other chosen signals. In Fig. 3.5 several signals and their spectral estimates are shown. There is obviously a large correlation between signals.

Fig. 3.6.a shows the statistics for the peak in the frequency domain for all 86 events, and Fig.3.6.b shows the corresponding histogram for estimation of the ice thickness using the theoretical approach and the 86 events from experimental hydrophone data. The rupture speed assume to be 1330 m/s.

3.5 The analysis of the second part of the signal.

The spectral analysis of the event # 61 is shown in Fig. 3.7. The first part of the event is the direct acoustic transmission from the crack into water (see section 1.1), and the later arrival is a dispersive flexural platewave. The nature of the second part of the signal is unclear. Note some facts:

1. dispersion (the high frequency components of the signal arrive at the receiver earlier than low components);

2. there is a wide peak in spectrum near 500 Hz.

My hypothosis is that the signal is the result of structural waves, which are propagating in the ice plate after cracking. The hydrophone is near the ice, so even subsonic waves can be considered. Application of the theory of elastic waves in solid plate to the Arctic Ice plate is considered in Chapter 4 for the explanation of the second part of the signal.

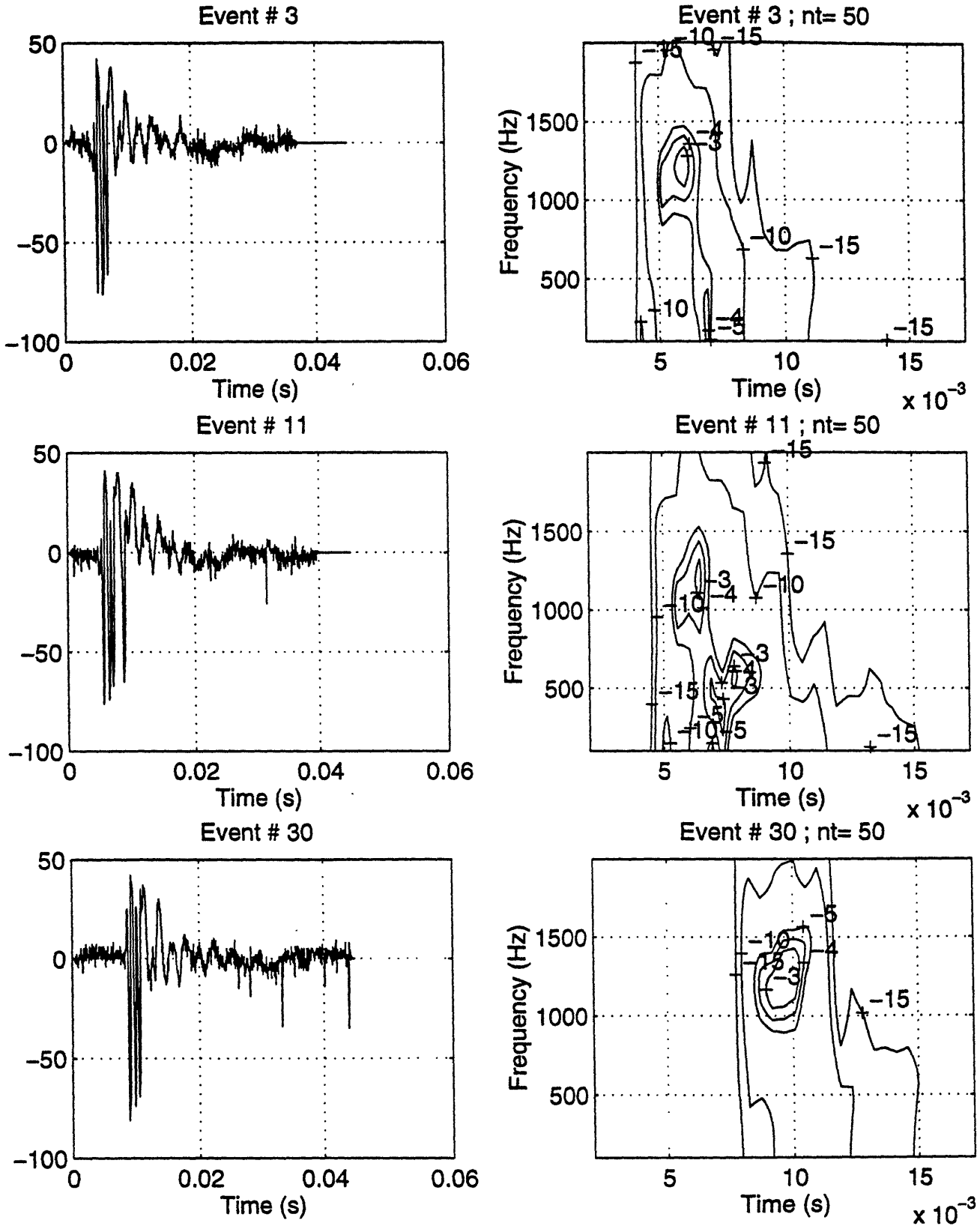

Figure 3-5: Sound-pressure time series for three events and the corresponding power spectral density in time-frequency domain.

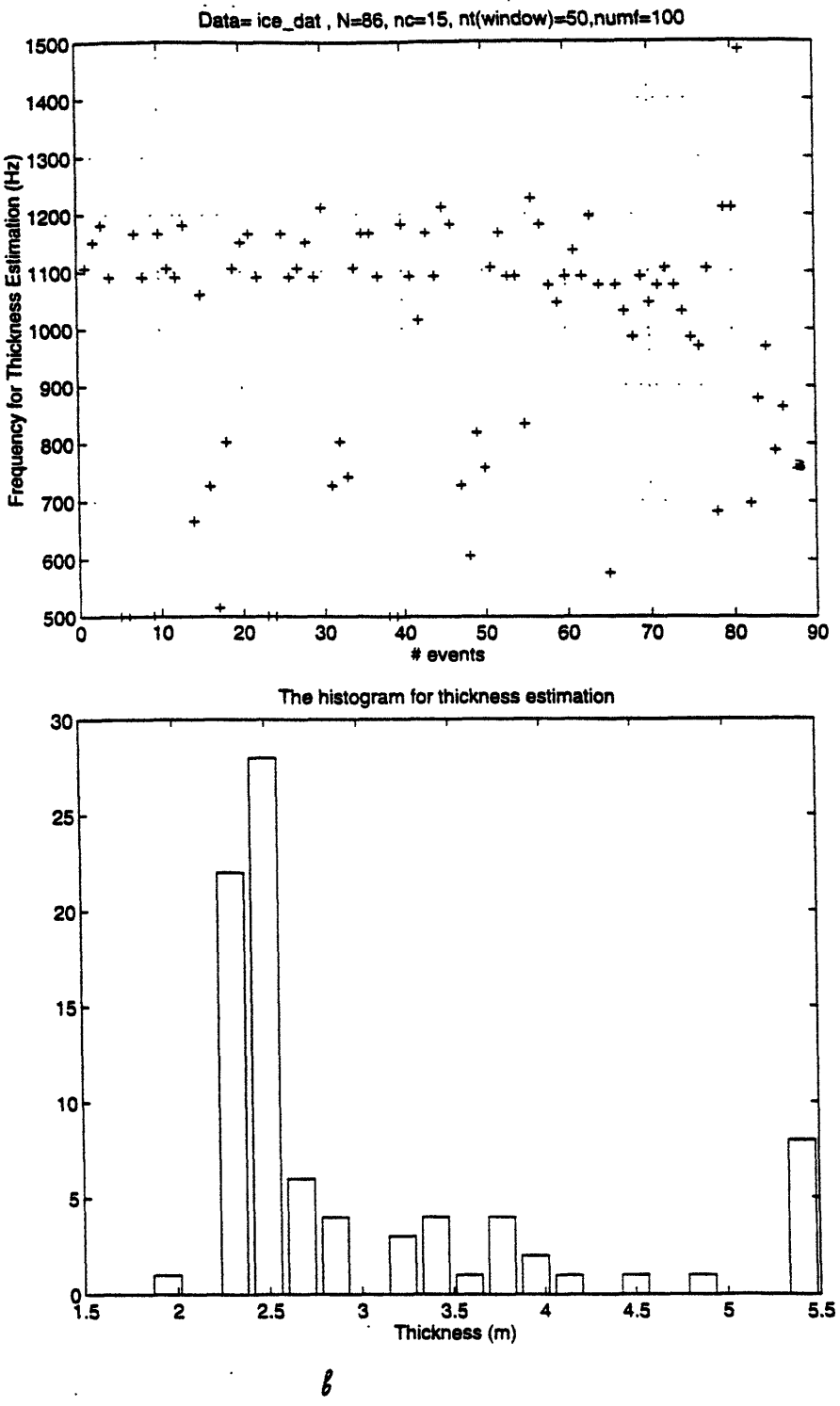

Figure 3-6: The estimation of the ice thickness based on the analysis of 86 events.

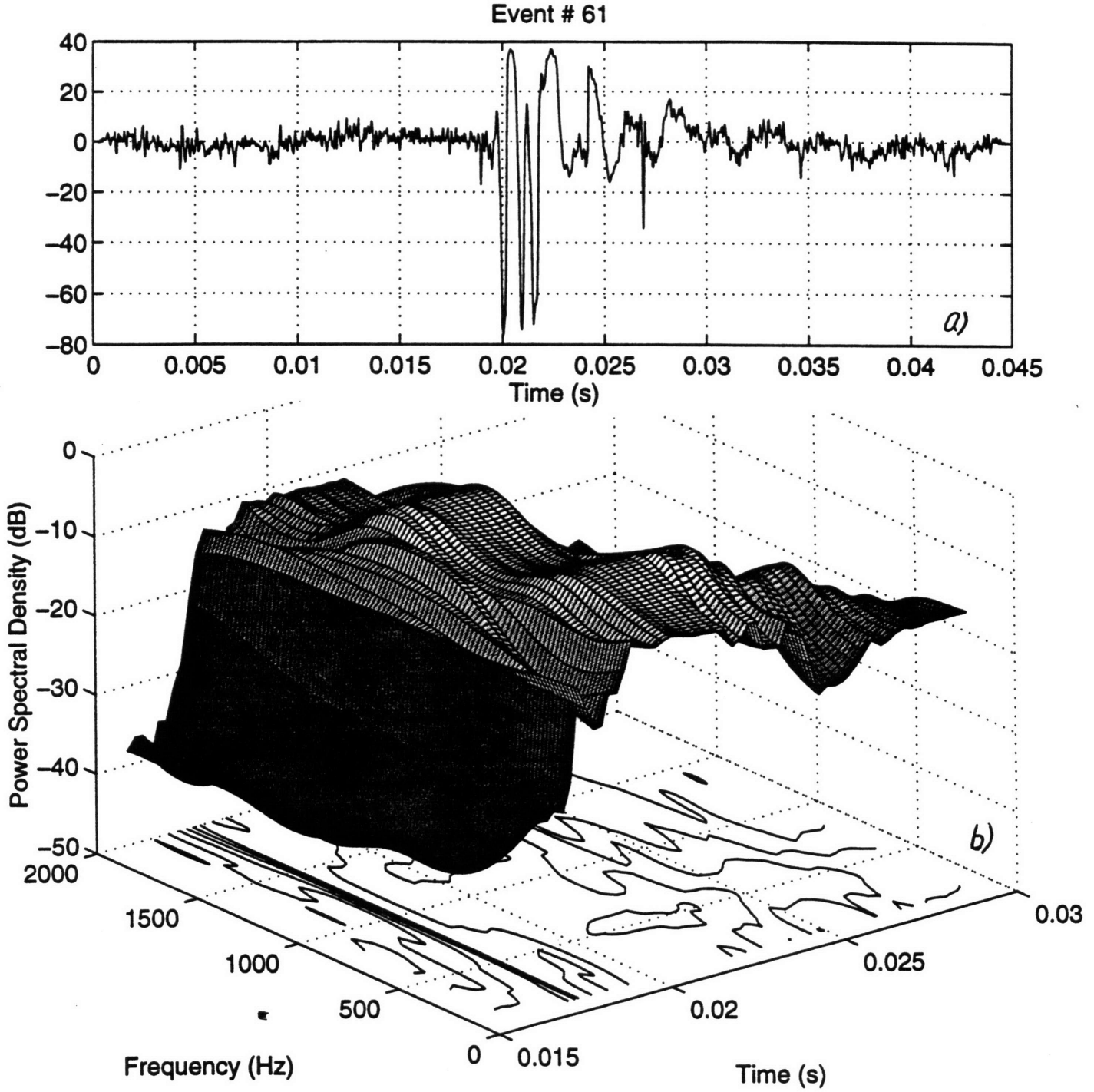

Figure 3-7: The analysis of the event # 61: (a) plot in time domain; (b) plot in time-frequency domain.

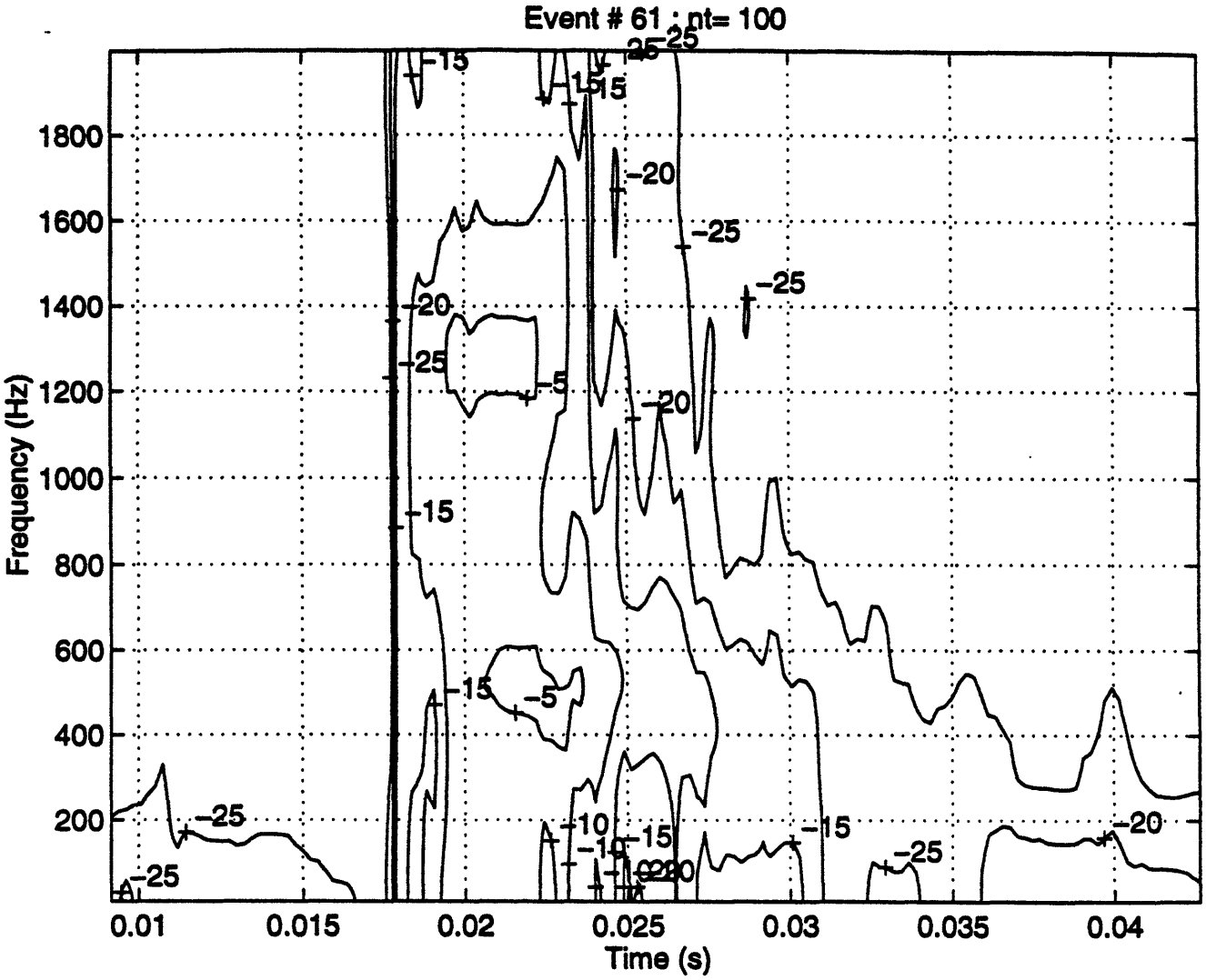

Figure 3-8: The analysis of the event # 61: contour plot in time-frequency domain

Chapter 4

Elastic waves in the Arctic ice plate

The sudden displacement at the fracture zone excites various elastic waves in the ice. Some of this energy, together with the directly transmitted signal, enters the water, and may contribute to the signal, analyzed in Chapter 3.

In this chapter the theory of elastic waves in an infinite solid plate is applied to the case of the Arctic ice plate. The goal is to establish analytically how elastic waves propagating in the ice plate contribute to the under-ice signal from a crack.

4.1 Theoretical considerations

4.1.1 Dispersion equation

Assume ice is an elastic material. For the first step of elastic waves in the ice plate research consider general case of structural waves in the elastic plate. *Lamb waves* refer to elastic perturbation propagating in a solid plate (or layer) with free boundaries, for which displacements occur both in the direction of wave propagation and perpendicularly to the plane of the plate.

Consider a plane harmonic wave propagating in a plate of thickness $h = 2d$ in the positive x direction (see Fig. 4.1). According to Ref. [20] the expressions for scalar

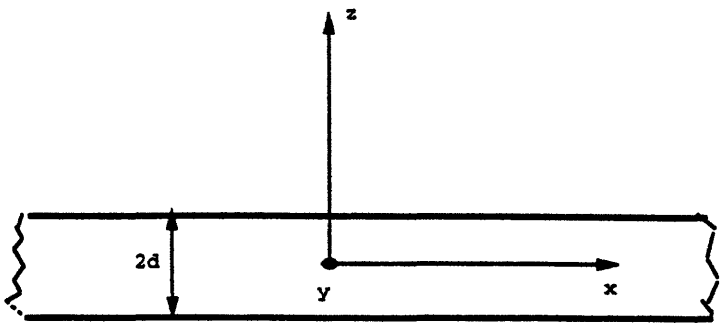

Figure 4-1: A solid plate and coordinate system

potential Φ and vector $\vec{\Psi}$ of the displacements, which are related to the particle displacements, is

$$\vec{v} = grad\Phi + rot\vec{\Psi}, \tag{4.1}$$

where $\vec{v}$ is the particle velocity. The potentials Φ and $\vec{\Psi}$, which describe longitudinal and transverse waves, respectively, must satisfy the wave equations:

$$\begin{aligned} \frac{\partial^2\Phi}{\partial x^2} + \frac{\partial^2\Phi}{\partial z^2} + k_l^2\Phi = 0, \\ \frac{\partial^2\vec{\Psi}}{\partial x^2} + \frac{\partial^2\vec{\Psi}}{\partial z^2} + k_t^2\vec{\Psi} = 0, \end{aligned} \tag{4.2}$$

where

$k_l = \omega\sqrt{\frac{\rho}{\lambda+2\mu}}$ is the wave number for longitudinal wave,
$k_t = \omega\sqrt{\frac{\rho}{\mu}}$ is the wave number for transverse wave,
ω is the circular frequency,
λ and μ are the elastic Lame constants, and
ρ is the density of the material of the plate.

The components U and W of the particle displacement along the x and z axes,

respectively, may be represent in terms of Φ and $\vec{\Psi}$ according to the equations:

$$U = \frac{\partial \Phi}{\partial x} - \frac{\partial \Psi}{\partial z},$$
$$W = \frac{\partial \Phi}{\partial z} + \frac{\partial \Psi}{\partial x}. \tag{4.3}$$

They also must satisfy the boundary conditions for free plate:

$$\sigma_{xy} \quad (z = \pm d) = 0, \tag{4.4}$$
$$\sigma_{zz} \quad (z = \pm d) = 0. \tag{4.5}$$

After solving wave equations (4.1) and satisfying boundary conditions for free plate Victorov in Ref. [20] and Cremer and Heckl in Ref. [21] obtained the *dispersion relation* for the phase speed of Lamb waves c and frequency ω:

$$[\frac{\tan\sqrt{1-s^2}\bar{d}}{\tan\sqrt{n^2-s^2}\bar{d}}]^{\pm 1} = -\frac{4s^2\sqrt{1-s^2}\sqrt{n^2-s^2}}{(1-2s^2)^2}, \tag{4.6}$$

where

$s^2 = \frac{c_t^2}{c^2}$ with c_t = the transverse waves speed,
$n^2 = \frac{c_t^2}{c_l^2}$ with c_l = the longitudinal waves speed,
$\bar{d} = k_t d$.

The equation (4.6) describes the dispersion curves for the two groups of waves each of which satisfies the wave equation of motion and the boundary conditions, i.e., both can propagate in the plate independently of one other.

The first group of waves, which corresponds to the +1 case in the left side of (4.6) describes waves in which the motion is symmetrical with respect to z =0 (i.e., the displacement U has the same signs, the displacement W opposite signs in the upper and lower halves of the plate).

The second group, which corresponds to -1 case, describes waves in which the motion is antysymmetrical with respect to z =0 (i.e., the displacement U has opposite

signs, the displacement W has the same sign in the upper and lower halves of the plate).

The waves of the first group are called symmetrical Lamb waves, those of the second group are called antisymmetrical.

4.1.2 Critical Frequencies

Consider the equation (4.6). The frequencies, which are roots of this equation for the case when the Lamb wave speed $c \longrightarrow \infty$ (or according to (4.6) $s \longrightarrow 0$), are called the *critical frequencies* for the plate with thickness $2d$.

For $c \longrightarrow \infty$ ($s \longrightarrow 0$) the right-hand side of the dispersion equation (4.6) is equal to zero; thus, such critical frequencies correspond to zeros (for symmetric modes) and poles (for antysymmetric modes) of tangent function in the numerator and satisfy the following equation:

$$\bar{d}_{cr} = \frac{\pi n}{2}, \tag{4.7}$$

where

n is any integer number, $n = 1, 2, 3...$,
$\bar{d}_{cr} = k_t d = \frac{2\pi f_{cr} d}{c_t}$, where f_{cr} is the critical frequency,
$d = \frac{h}{2}$, where h is the plate thickness,
c_t is the transverse wave speed for plate material.

After these simple calculations are evaluated the expression for critical frequencies of the Lamb waves is

$$f_{cr} = \frac{c_t n}{2h}, n = 1, 2, 3, ... \tag{4.8}$$

Note that $n = 1, 3, 5...$ correspond to anti-symmetric modes, and $n = 2, 4, 6...$ correspond to symmetric modes.

4.1.3 Attenuation of Lamb Waves as a Function of Frequency.

The presence of dispersion in the phase and group velocities of Lamb waves has an important effect on the behavior of the attenuation factor for these waves. In regions of strong phase velocity dispersion, the attenuation exhibits a rather steep dependence on the frequency and thickness of the plate, i.e., on $k_t d$.

For the calculation of the indicated dependences, Viktorov (in Ref.[20]) specifies the attenuation of longitudinal and transverse waves in the solid medium as the imaginary parts of the corresponding wave numbers:

$$\begin{aligned} \bar{k}_l &= k'_l + ik''_l, \\ \bar{k}_t &= k'_t + ik''_t, \\ \bar{k}_{s_n,a_n} &= k'_{s_n,a_n} + ik''_{s_n,a_n} \end{aligned} \tag{4.9}$$

Assume the attenuation of transverse and longitudinal waves is small: $k'_l >> k''_l$ and $k'_t >> k_t{}'$). The attenuation of all Lamb waves in this case is also small, except *in the vicinity of the critical points.* The complex wave numbers for the longitudinal, transverse, and n-th order symmetrical and antisymmetrical Lamb waves may be rewritten in the different form:

$$\begin{aligned} \bar{k}_l &= k'_l(1 + i\alpha), \\ \bar{k}_t &= k'_t(1 + i\beta), \\ \bar{k}_{s_n,a_n} &= k'_{s_n,a_n}(1 + i\gamma_{s_n,a_n}), \end{aligned} \tag{4.10}$$

where

$\alpha = k''_l / k'_l,$

$\beta = k''_t / k'_t,$

$\gamma = k''_{s_n,a_n} / k'_{s_n,a_n},$

are small real corrections, numerically equal to the attenuation factors, divided by 2π, for longitudinal, transverse, and Lamb waves per corresponding wavelength. To evaluate the relationship between α, β and γ the next steps have to be done:

1. substitute the complex wave numbers into the characteristics equations (see Ref. [20])
2. reject terms of order α^2, β^2, γ^2 and higher,
3. separate the equations into their real and imaginary parts. (The real parts yield equations determining the phase velocities of the Lamb waves, the imaginary parts yield equations for the attenuation factors.)

From this routine Victorov obtains the following expressions:

$$\gamma_{s_n} = A_{s_n}\alpha + B_{s_n}\beta,$$
$$\gamma_{a_n} = A_{a_n}\alpha + B_{a_n}\beta, \tag{4.11}$$

where A_{s_n}, B_{s_n}, A_{a_n} and B_{a_n} depend on $\bar{d}$, s and n. I don't include here the expressions and corresponding figures for these coefficients, they can be found in Ref. [20]. I would like to make one important note for this research common property. As a rule, the attenuation of Lamb waves is a maximum when the phase velocity dispersion is a maximum. For example, in the critical regions, when the phase velocities and wave lengths tend to infinity, the attenuation factors γ_{s_n,a_n} also tend to infinity.

4.2 The dispersion equation solutions for the Arctic Ice plate

The equation (4.6) is the dispersion equation for Lamb waves in an elastic plate. Many authors have performed calculations of the phase and group velocities and their dependence on the plate thickness and frequency (dispersion curves). One of such solutions (Ref. [20]) for the dimensionless coordinates c/c_t and $k_t d$ are shown in Fig 4.2.

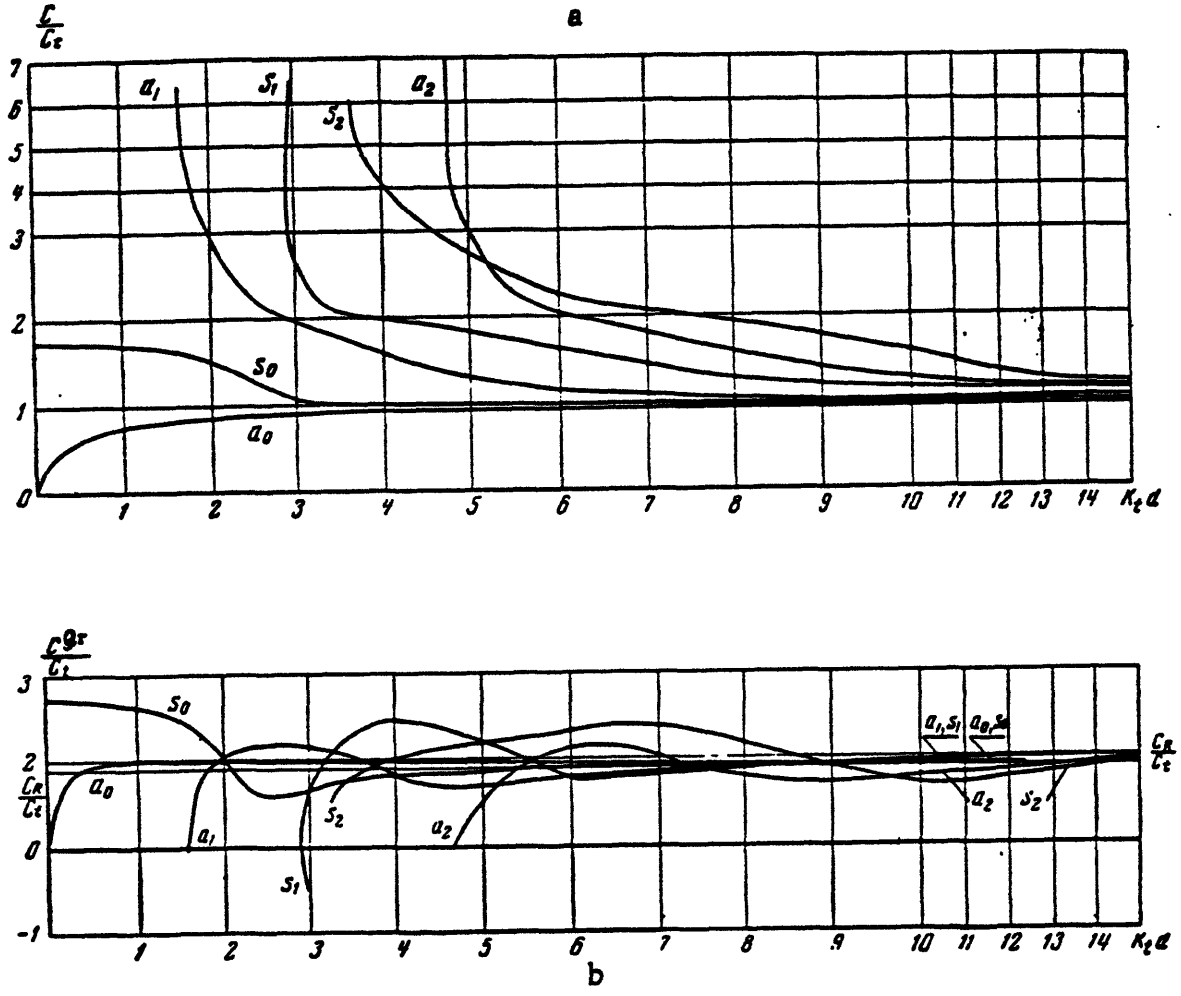

Figure 4-2: Dispersion diagram for free plate waves: symmetric and antisymmetric modes. A Poisson ratio $\nu = 0.34$ is used. (From Ref.[20])

In this section the numerical solutions of symmetric and antysymmetric modes for ice sheet is considered. The goal of this theoretical anlysisis to explain some spectral properties of the ice cracking data, which were noted in Chapter 3.

4.2.1 The method of solving

To compute the dispersion curves for the Arctic ice plate and view the phase velocity-frequency plot the method of solving the dispersion equation (4.6) and the computer program (MATLAB) were created.

The method includes the following assumptions and notes:

- Assume that the ice plate is in vacuum. The boundary conditions (1.4) holds.
- Assume that the phase velocities of longitudinal and transverse waves in the ice are known and equal 3100 m/s and 1750 m/s respectively.
- The dispersion equation has two unknowns: the phase velocity of Lamb waves c and frequency f.
- Right-hand side includes only one variable c

This allows us to do calculations as follows:

1. Chose the frequency band of interest

$$f = [f_1 f_2 f_3 \ldots f_n]. \tag{4.12}$$

2. Calculate the right-hand side

$$RS = -\frac{4s^2\sqrt{1-s^2}\sqrt{n^2-s^2}}{(1-2s^2)^2}, \tag{4.13}$$

where

$s^2 = \frac{c_t^2}{c^2}$ with c_t = the transverse waves speed,
$n^2 = \frac{c_l^2}{c_t^2}$ with c_l = the longitudinal waves speed,

for all frequencies f:

$$RS = [RS(f_1)RS(f_2)RS(f_3)...RS(f_n)]. \tag{4.14}$$

3. Chose the array of phase velocity values:

$$c = [c_1c_2c_3...c_m]. \tag{4.15}$$

4. For each c_i

   - calculate left-hand side of the dispersion equation

$$LS = [\frac{\tan\sqrt{1-s^2}\bar{d}}{\tan\sqrt{n^2-s^2}\bar{d}}]^{\pm 1} \tag{4.16}$$

     to get

$$LS(c_i) = [LS(f_1, c_i)LS(f_2, c_i)LS(f_3, c_i)...LS(f_n, c_i)]; \tag{4.17}$$

   - find $f_j = f_{result}$, for which

$$|RS(f_j) - LS(f_j, c_i)| \tag{4.18}$$

     is small;

   - (f_{result}, c_i) is a point on one of the dispersion curve (or one of solution of the dispersion equation);

5. Note that for the case of choosing arrays c and f such that the RS and LS are real, it is better use another test:

$$(RS(f_j) - LS(f_j, c_i))(RS(f_{j+1}) - LS(f_{j+1}, c_i)) < 0 \tag{4.19}$$

for the estimation of frequency-root of the equation for $c = c_i$ (See Fig. 4.3).

6. In the most cases of c_i there are more then one point for frequency f : $f_{result1}$, $f_{result2}$, $f_{result3}$..., where RS and LS have crossing. These cross points correspond to different modes or, graphically speaking, dispersion curves.

4.2.2 The results of calculation: symmetric and antisymmetric modes.

The calculations were provided for c_l =3100 m/s and c_t =1750 m/s.

There are two different cases of the dispersion equation for Lamb waves. The first is

$$\frac{\tan\sqrt{1-s^2}\bar{d}}{\tan\sqrt{n^2-s^2}\bar{d}} = -\frac{4s^2\sqrt{1-s^2}\sqrt{n^2-s^2}}{(1-2s^2)^2}. \tag{4.20}$$

This equation corresponds to the symmetrical Lamb waves. The numerical solution is shown in Fig. 4.4.

The second is

$$\frac{\tan\sqrt{1-s^2}\bar{d}}{\tan\sqrt{n^2-s^2}\bar{d}} = [-\frac{4s^2\sqrt{1-s^2}\sqrt{n^2-s^2}}{(1-2s^2)^2}]^{-1}. \tag{4.21}$$

This equation corresponds to the antisymmetrical Lamb waves. The numerical solution is shown in Fig. 4.5.

Note that the results of calculations consist well with the previous numerical solutions. (One of them, shown on Fig.4.1, is from Viktorov's book, and second may be find on p.163 of Ref.[21]). It allows to say that the program for equation solving works.

4.2.3 Dispersion of phase and group speed in 100-1000 Hz frequency segment

Consider the zeroth antysymmetric mode. It is the most important mode for the cracking in-water detected event because the curve is in [1000 – 1600] m/s phase velocity band for the frequency [100 – 1000] Hz. (See Fig. 4.6)

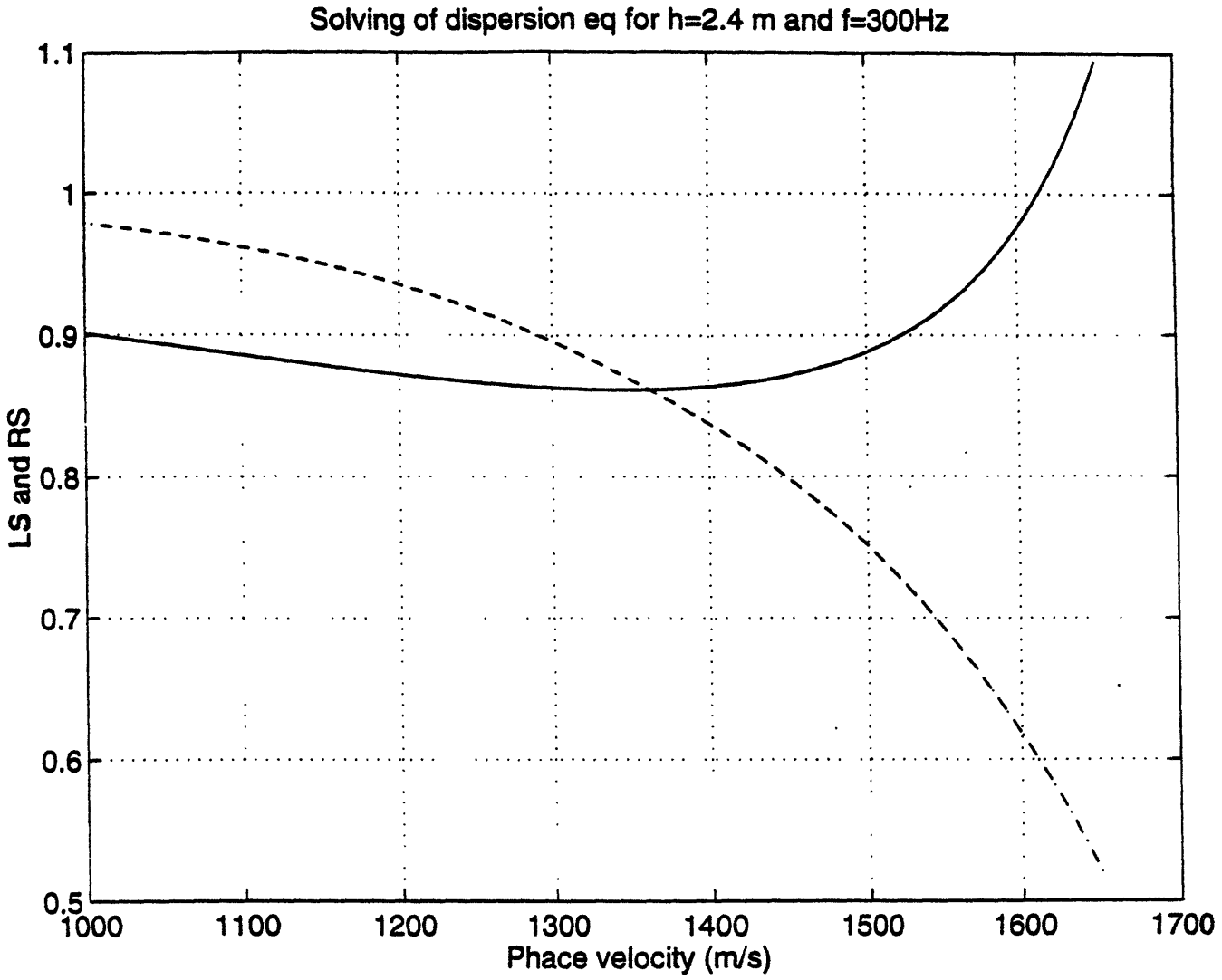

Figure 4-3: Graphical demonstration of dispersion equation solving for antisymmetric modes; the frequency $f = 300$Hz. Solid line is for the right side of the equation, and dashed is for left side.

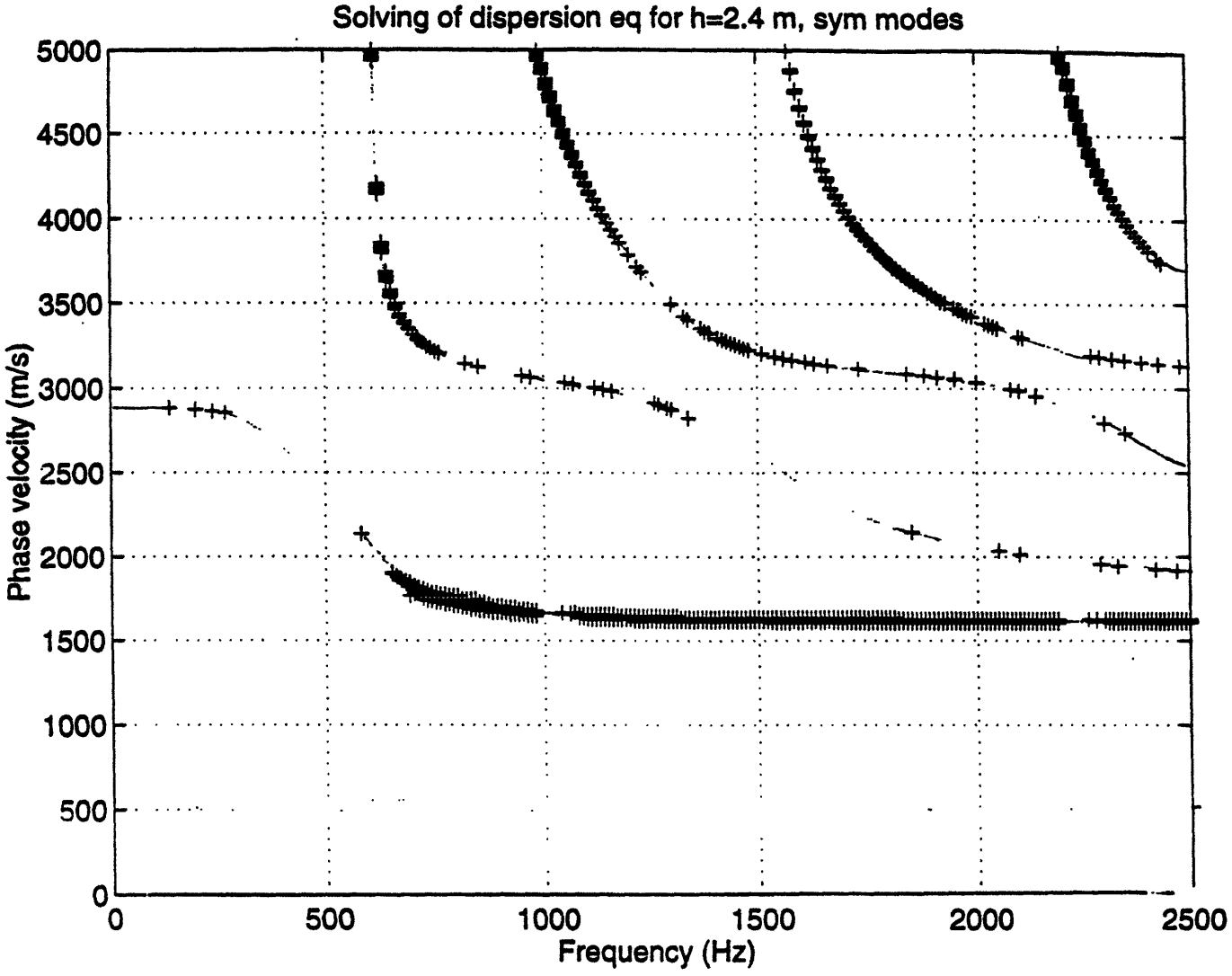

Figure 4-4: The dispersion curves for symmetrical modes for ice plate with $h = 2.4$ m

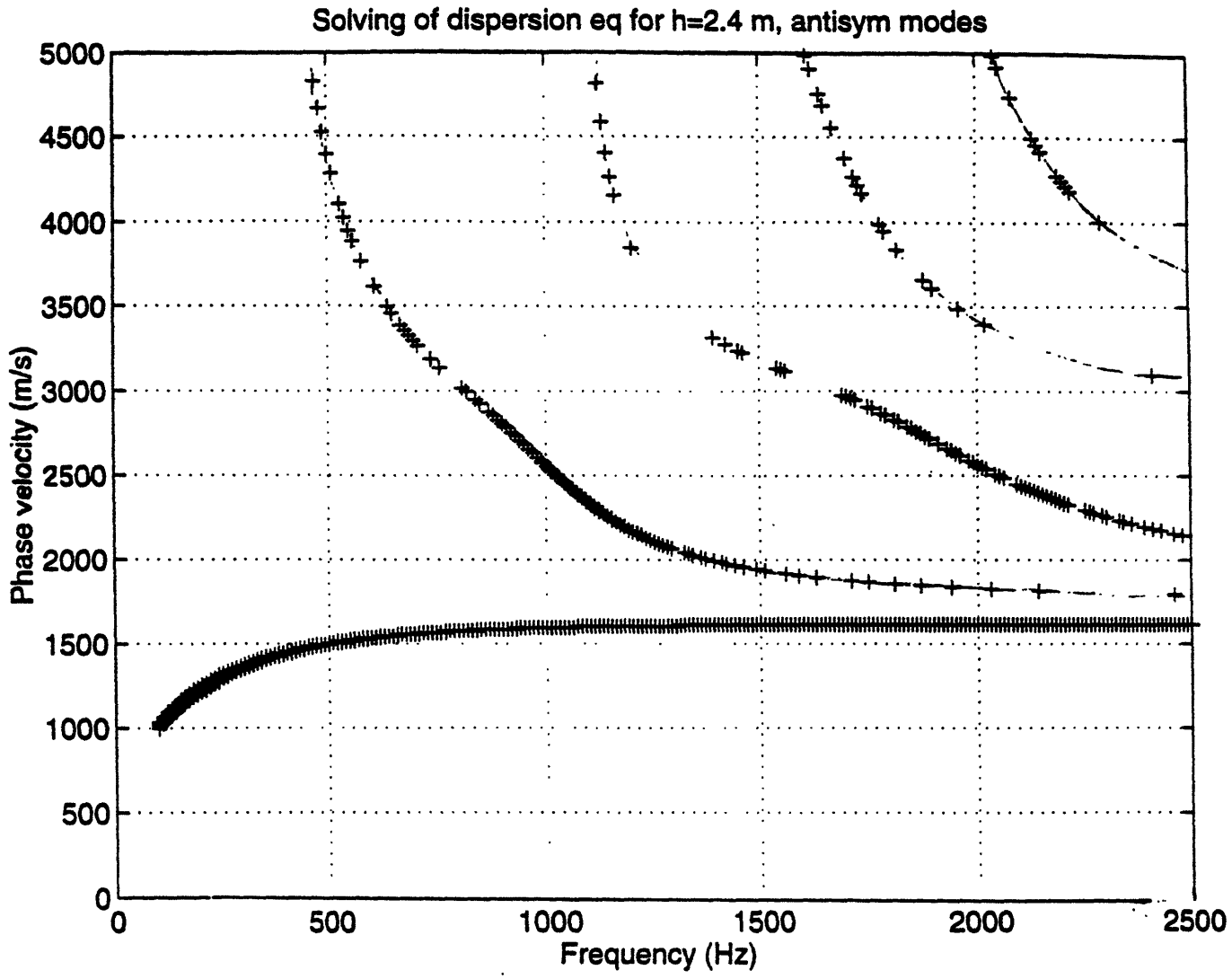

Figure 4-5: The dispersion curves for antisymmetrical modes for ice plate with $h = 2.4$ m

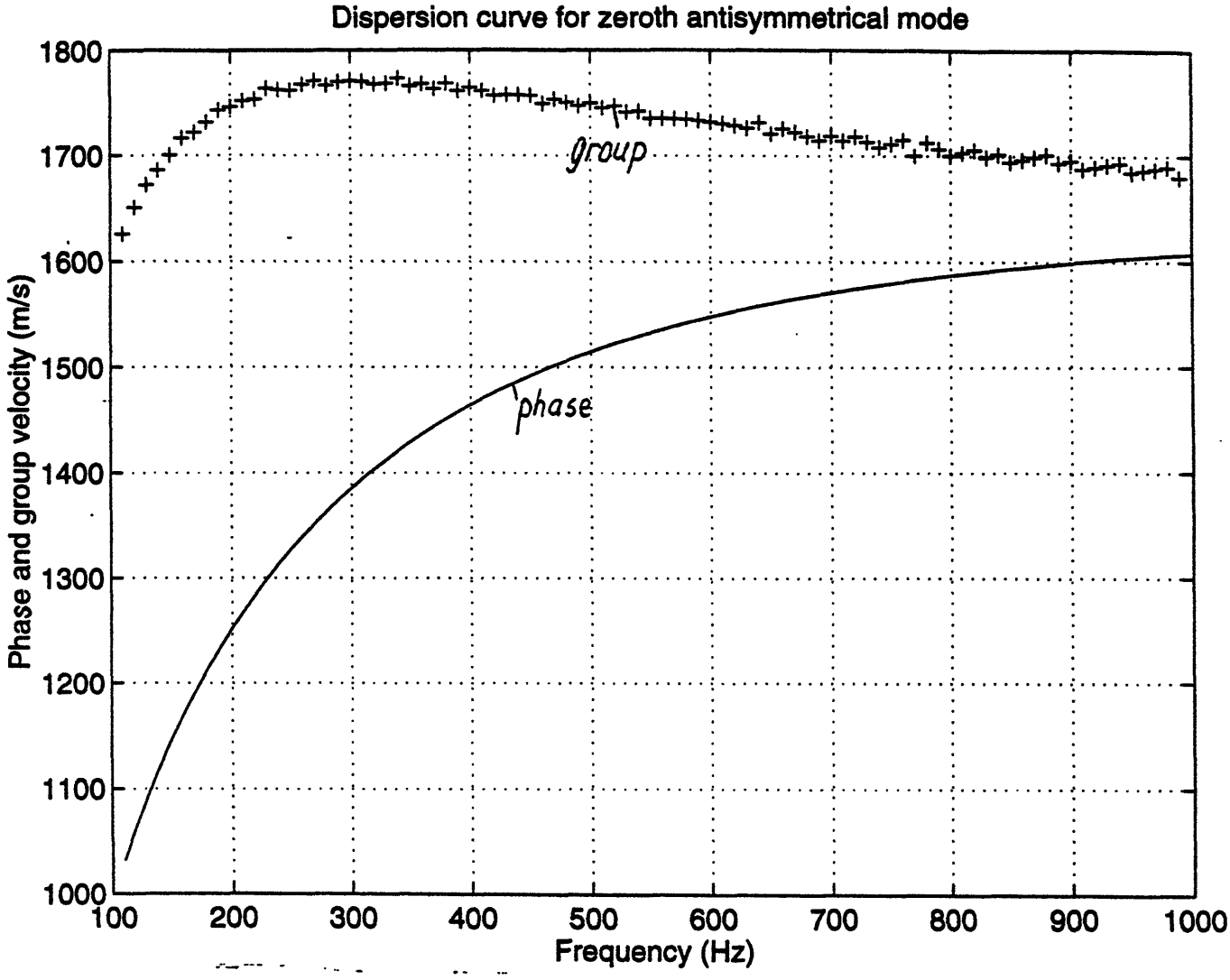

Figure 4-6: Phase and group speed like function of frequency for zeroth antysymmetric mode with $h = 2.4$ m

The group velocity curve is also calculated. These velocities may be determined from the solutions for phase velocity in view of:

$$c_{gr} = \frac{d\omega}{dk} = \frac{c}{1 - \frac{\omega}{c}\frac{dc}{d\omega}} = \frac{c}{1 - \frac{f}{c}\frac{dc}{df}}. \tag{4.22}$$

Fig. 4.7 shows that the values of group velocity for zeroth antysymmetric mode are 1300-1750 m/s. It means that these waves come to the point of the receiver in the same time of the waterborne signal, so they contribute to the recording events. The effect of Lamb waves dispersion in terms of phase and group velocities, as well as arrival time at the hydrophone location is shown on Fig.4.7 and 4.8. It can explain the effect of dispersion in the second part of the events. (See Fig. 3.8) Both the supersonic and subsonic cases may be considered because the receiver is close to the ice plate.

4.3 The attenuation of the Lamb waves in the ice plate

It is noted above that the attenuation factors for the Lamb waves are dispersive. They depend on $\bar{d}, s$ and n for each mode.

The attenuation of Lamb waves is a maximum when the phase velocity dispersion is a maximum. Therefore, for analysis of attenuation of Lamb waves as a function of frequency in the ice sheet, first, consider the dispersion curves for both symmetrical and antisymmetrical modes which occurs in the [100...1000] Hz frequency band for 2.4 m ice thickness case. The numerical dispersion equation solution of this case is given in Fig. 4.9. According to the picture there are four modes in this frequency band: zeroth symmetrical, zeroth antysymmetrical, first symmetrical, and first antysymmetrical.

Like it is noted above in Section 4.1, theoretically, the attenuation factors γ_{s_n,a_n} tend to infinity in the critical regions. It means that we may expect the lower amplitude of power spectral density of the signal in these critical regions.

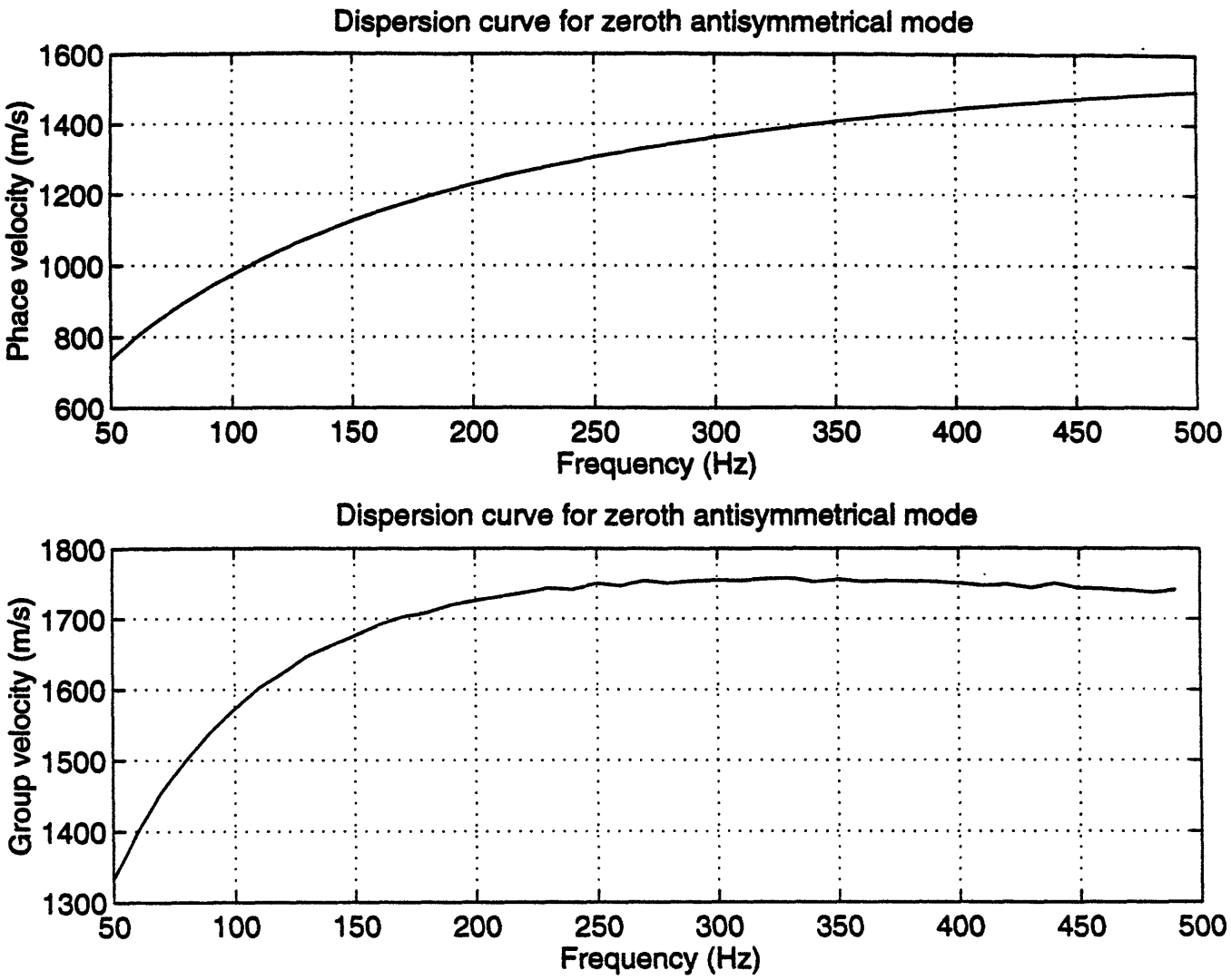

Figure 4-7: The dispersion effect for zeroth antysymmetrical mode for ice plate with $h = 2.4$ m (phase and group speed)

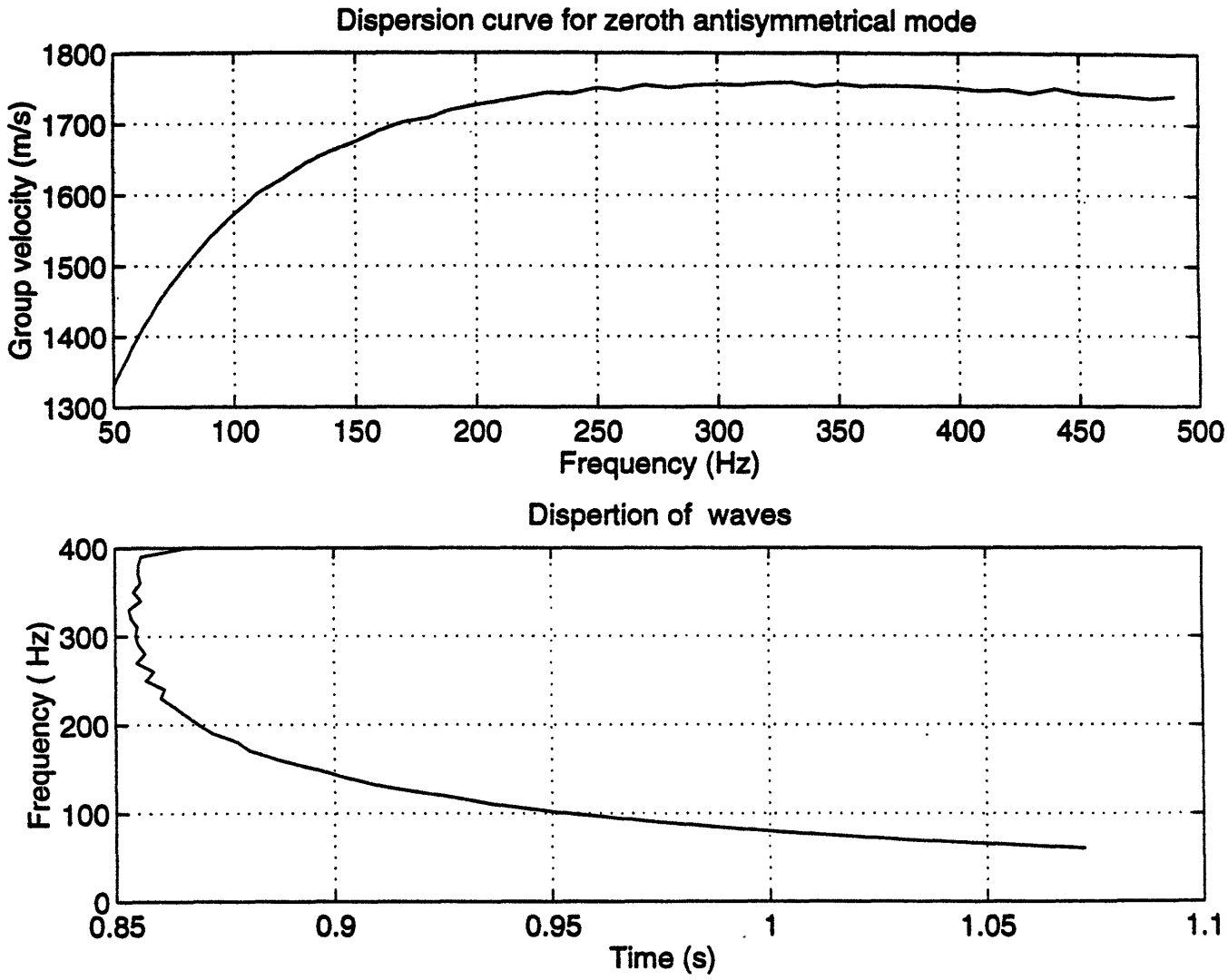

Figure 4-8: The dispersion effect for zeroth antysymmetrical mode for ice plate with $h = 2.4$ m (group speed and arriving time)

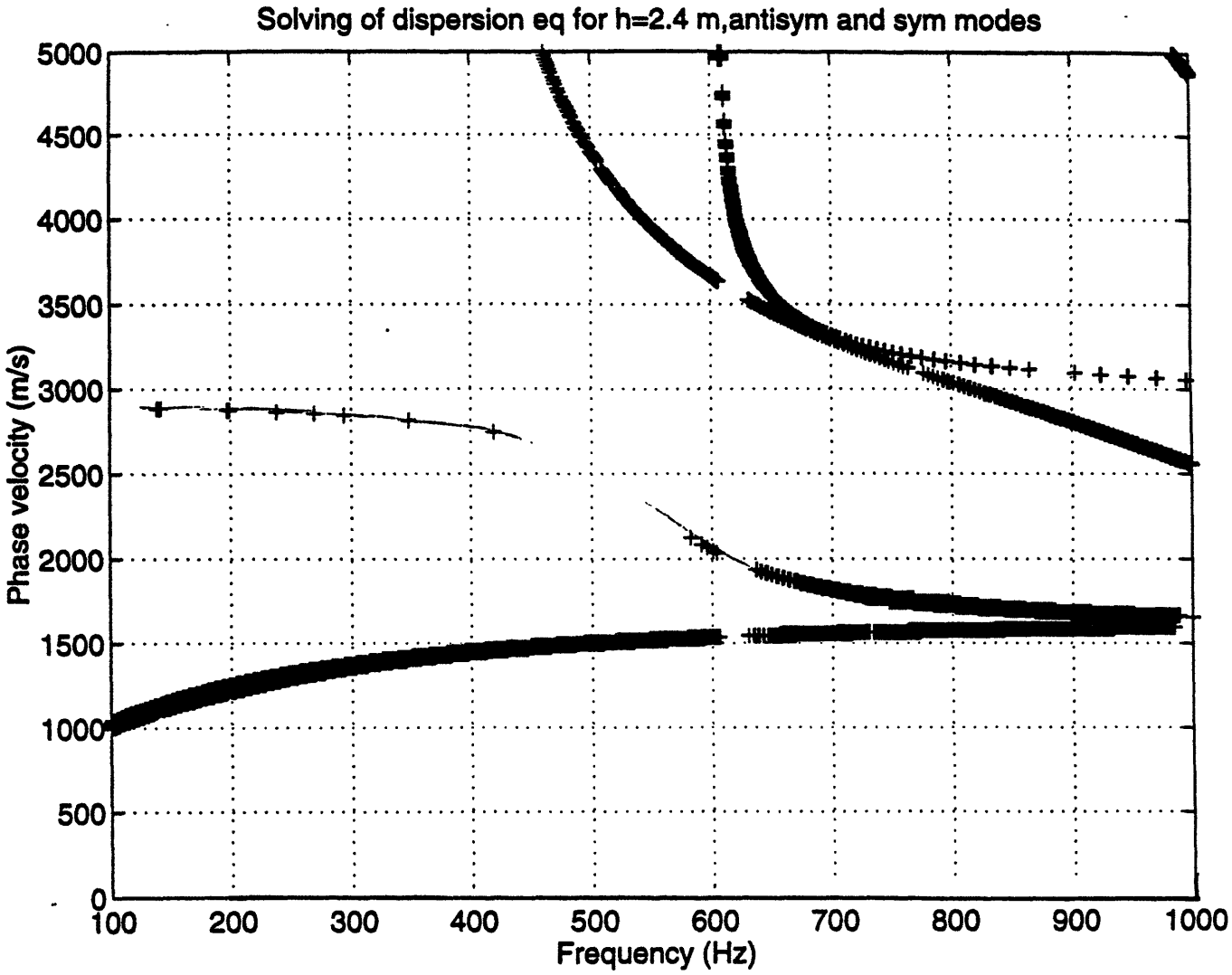

Figure 4-9: The symmetrical and antysymmetrical curves for ice plate with $h = 2.4$ m

The critical frequencies according to (4.8) are

$$f_{cr} = \frac{c_t n}{2h}, n = 1, 2, 3, ... \tag{4.23}$$

In the frequency band of interest there are two critical frequencies:

$$f_{cr1} = \frac{1750 \cdot 1}{2 \cdot 2.4} = 364.5(Hz); f_{cr2} = \frac{1750 \cdot 2}{2 \cdot 2.4} = 730(Hz). \tag{4.24}$$

These considerations may explain the peak near approximatly 500 Hz in the experimental data for a cracking event. (See Fig.3.8)

In summary, I note that the values of the critical frequencies for the ice plate correlate with ice thickness. (See Eq. (4.23)) If we assume that the transverse waves speed is constant for the regions with different thickness, the peak frequency in the second part of the signal increase with h becomes less. So both peaks (in the first and the second part of the signal) go up along frequency axis when ice become thicker.

Chapter 5

Conclusions

The value of ice thickness can be estimated from the ambient noise under the ice plate. For the approach described in the thesis one needs to record the pressure field data with the following recommendations:

- The recorded data should include a time segment when significant cracking occurs.
- One hydrophone is needed for each research area.
- The hydrophone should be placed approximately at a depth of 5 m under the ice plate.
- The frequency range for the recording is 10 Hz to 10 kHz.

Data analyzing process includes the next steps. There are many events relatively large compared with the average noise amplitude. For ice thickness estimation we need the events which are from propagating cracks. (The methods of sorting events into two categories: "good" (from propagating cracks) and "bad" (all others) are not established in the thesis.) Geophone data or correlation test with previously recorded propagating events (see Chapter 3) may be used for the classification process.

- The first part of the event (Fig. 3.7) is the point of interest for the ice thickness estimation.

- The relationship between the frequency in which the peak in the power spectrum density occurs and ice thickness is based on the theory described in Chapter 2.

For the testing of this theory the experimental hydrophone data collected in the Beaufort Sea during the spring of 1994 were used. The spectral analysis of the events demonstrates the presence of the peak, $f_0 \approx 1150$ Hz, which correlates well with the measured ice thickness $h \approx 2.5$ m at the site.

But one test is not enough. I recommend to develop more experiments with the hydrophone data of under ice noise for areas of the Arctic ice with different thickness. It would be possible after that to establish the relationship between f_0 and h. In reality it may not be so simple as described by analytical model (see expression (2.32)).

Another important result described in the thesis is that elastic waves, which propagate in the ice, also contribute to the ambient noise events from propagating cracks. For a given or estimated value of ice thickness the critical frequencies may be calculated. The attenuation of Lamb waves depends on frequency. In the critical regions the attenuation factors γ_{s_n,a_n} (for symmetric and antisymmetric modes) tend to infinity theoretically, so they should have maximum peaks for real data. Therefore we can expect maximum peak in the power spectral density function in the region between the critical frequencies, which was observed in Beaufort Sea data.

Bibliography

[1] James K. Lewis and Maria R. Giufrida. Sea-Ice Kinematics as Determined by Remotely-Sensed Ice Drift: Seasonal Space and Time Scales. *Photogrammetric Engineering and Remote Sensing*, Vol.55, No.8, August 1989, pp. 1113-1121.

[2] James K. Lewis, Randy D. Crissman and Warren W. Denner. Estimating Ice Thickness and Internal Pressure and Stress Forces in Pack Ice Using Lagragian Data.*Jornal of Geophisical Research*, Vol.91, No. C7, July 15,1986, pp.8537-8541

[3] James K. Lewis. Relating Arctic Ambient Noise to Thermally-Induced Fracturing of the Ice Pack.

[4] P.J. Stein. Acoustic Monopole in a Floating Ice Plate. PhD thesis, Massachusetts Institute of Technology, Feb. 1986.

[5] A.J. Langley. Acoustic Emission from the Arctic Ice Sheet.*J. Acoust. Soc. Am.*, Vol 85, 1989, pp.692-701.

[6] J.S. Kim. Radiation from Directional Seismic Sources in Laterally Stratified Media with Aplication to Arctic Ice Cracking Noise. PhD thesis, Massachusetts Institute of Technology, May 1989.

[7] I. Dyer. The Song of Sea Ice and other Arctic Ocean Melodies.*Arctic Technology and Policy.* Hemisphere, Washington, DC, 1983, pp. 11-37.

[8] A.R. Milne, Thermal Tension Cracking in Sea Ice: A Source of Underice Noise.*J.Geophys.* Res.77, 1972, pp.2177-2192.

[9] David M. Farmer and Yunbo Xie. The Sound Generated by Propagation Cracks in Sea Ice.*J. Acoust. Soc. Am.* 85 (4), April 1989.

[10] C.F. Chen, S. J. Merz, and I. Dyer. Analysis of Marginal Ice Zone Noise Events. Department of Ocean Engineering, MIT.

[11] N.A. Haskell, Total Energy and Energy Spectral Density of Elastic Wave Radiation from Propagating Faults.*Bull Seismol. Soc. Am.* 54, 1964, pp. 1811-1841.

[12] J.C. Savage. Relation of Corner Frequency to Fault Dimensions.*J. Jeophys.* Res. 77(20), 1972, pp. 3788-3795.

[13] M. Ohnaka, Y.Kuwahara, K. Yamamoto, and T. Hirasawa. Dynamic breakdown processes and the generating mechanism for high frequency elastic radiation during stick-slip instabilities. *Earthquuake Source Mechanics*, American Geophysical Monograph 37, 1986.

[14] T.L.Paxson and R.A.Lucas. Experimental investigation of the velocity characteristics of a fixed boundary fracture model. *Dynamic Crack Propagation.* Noordhoff International Publishers, 1973.

[15] L. Mansinha, the Velocity of Shear Fracture, *Bull. Seismol. Soc. Am.* Vol. 54, 1964, pp. 369-376.

[16] W. M. Ewing, W.S. Jardetzky, and F. Press, *Elastic Waves in Layered Media*, McGraw-Hill, New York, 1957, pp. 281-327.

[17] B.E. Miller, H. Schmidt. Observation and inversion of seismo-acoustic waves in a complex arctic ice environment. *J. Acoust. Soc. Am.* Vol. 89(4),Pt.1,April 1991.

[18] S.M. Kay, S.L. Marple, Jr, Spectrum Analysis-A Modern Perspective. *Proceeding of the IEEE*, Vol.69, No.11, 1981, pp. 1380-1419.

[19] L.C. Posey. High resolution spectral estimates, Lincoln Laboratory, MIT, Tech. Note 1975, Jan 21, 1975.

[20] I.A. Viktorov. *Rayleigh and Lamb Waves.* Plenum Press, New York, 1957.

[21] L.Cremer, M. Heckl, *Structure-Borne Sound.* Stringler Verlag, New York, and Heidelberg, Berlin, 1973.